SGP-TR-205

Evaluation of DNA-Embedded Silica Nanoparticle Tracers

Timothy Spencer Manley

June 2015

Financial support was provided through the
Department of Energy Resources Engineering,
Stanford University

Stanford Geothermal Program
Interdisciplinary Research in
Engineering and Earth Sciences
STANFORD UNIVERSITY
Stanford, California

Abstract

Potential nanoparticle tracers were evaluated for durability at high geological temperatures and during transport through porous media. Nanoparticle tracers are an application of nanotechnology that could have very important applications to the energy industry. Much of the complexity involved in petroleum and geothermal operations revolves around the uncertainty with which one can characterize a reservoir of interest. Existing tools are confined largely to the wellbore, which requires much of the analysis to be inferred from indirect measurements. Nanoparticle tracer technology could enable measurements from within the reservoir, thereby removing a large degree of uncertainty. These sensors could be configured to collect information about the heating or flow characteristics of a geothermal reservoir, or to identify leakage of a hydraulic fracturing operation into surrounding aquifers.

Silica was investigated as a potential "shell" to carry nanoparticle sensors. Existing research (Ames, 2011; Alaskar, 2013) indicated that silica spheres have very robust flow characteristics. It has also been demonstrated (Paunescu et al., 2012, 2013; Puddu et al., 2013) that synthetic DNA could be successfully adsorbed onto charged silica nanoparticles, which were subsequently coated with another layer of silica to preserve the DNA in a fossil-like state. These nanoparticles were subjected to temperatures up to 200°C for 15 minutes, and sufficient DNA remained for unequivocal identification.

The advantage of DNA is its uniquely identifiable nature, which allows for individual particles to be tagged in a way that guarantees their origin. In addition, the spherical silica nanoparticle shell has a distinct appearance under SEM (Scanning Electron Microscope) in comparison to sand fines, which are often coarse. When suspended in liquid water, the particles are invisible to the human eye.

The first set of experiments tested solid silica nanoparticles during heating at 198°C for varying lengths of time up to 25 minutes. The second set of experiments flowed solid silica nanoparticles through packed sand at 25°C, 120°C, and 150°C while monitoring permeability changes. The final experiment flowed silica nanoparticles carrying synthetic DNA, which had been adsorbed onto a seed and coated with silica for protection. For all experiments, nanoparticles were sampled and subsequently analyzed with SEM imaging.

Acknowledgments

First of all, I would like to thank Roland Horne for his expert guidance and support. I would also like to thank members of the Stanford Geothermal Program for their research advice and friendship. Thanks to Maytham Al Ismail, Adam Jew, Chuck Hitzman and Kewen Li for their advice and assistance with lab equipment. Thanks to Morgan Ames, Jack Norbeck, Anna Suzuki, Carla Co, Yang Wong, Halldora Gudmundsdottir and Renfeng Jiang for sharing their insights in our weekly meetings. Thanks to Yuran Zhang for synthesizing the silica nanoparticles used in most of my experiments.

My heartfelt thanks go to my family for their unconditional love and support. I would like to thank my parents, Tim and Jennifer Manley, my siblings, Kara and Alex, my grandparents, Vance and Maxine Walker and Maurice and Jean Manley, and Lauren for their encouragement and faith in my potential.

Some of the information in this report has appeared in a similar form in the co-authored paper entitled "DNA-Encapsulated Silica Nanoparticle Tracers for Fracture Characterization" by Zhang and Manley, 2015.

Contents

List of Tables

List of Figures

Chapter 1

1. Introduction

1.1. Particle Tracers

In order to characterize flow networks within a reservoir more accurately, tracers have been utilized in both geothermal and petroleum applications. Data analysis typically involves simultaneous sampling of wells in the same field, with the intention of catching the "breakthrough curve" of the injected tracer. As breakthrough may not occur until months or years after injection, field tests require breakthrough estimates and continuous monitoring. There are several types of tracers, and each has a drawback. Some are radioactive, some decay in the reservoir, and some can occur in nature and may confuse the data analysis.

As opposed to more common chemical tracers, particle tracers could be utilized to carry sensors. The most obvious downside is the difficulty in transport. Particle tracers must be small enough to travel through the pore space of the reservoir. This means that they must remain in suspension, experience little or no aggregation, and avoid interactions with the rock matrix they are passing through (Kanj et al., 2009). The ability to construct nanoparticles and observe them under SEM (Scanning Electron Microscope) has opened a nanotechnology sector in the field of particle tracers.

Silica nanoparticle tracers were investigated because of their ability to carry information inside a silica "shell," which is an ideal spherical shape with a diameter that can be fabricated to a specific size. Extensive research has been conducted by Paunescu et al. (2012, 2013) to demonstrate the feasibility of silica nanoparticles as a carrier for synthetic DNA. This process was replicated by labmate Yuran Zhang (Zhang and Manley, 2015).

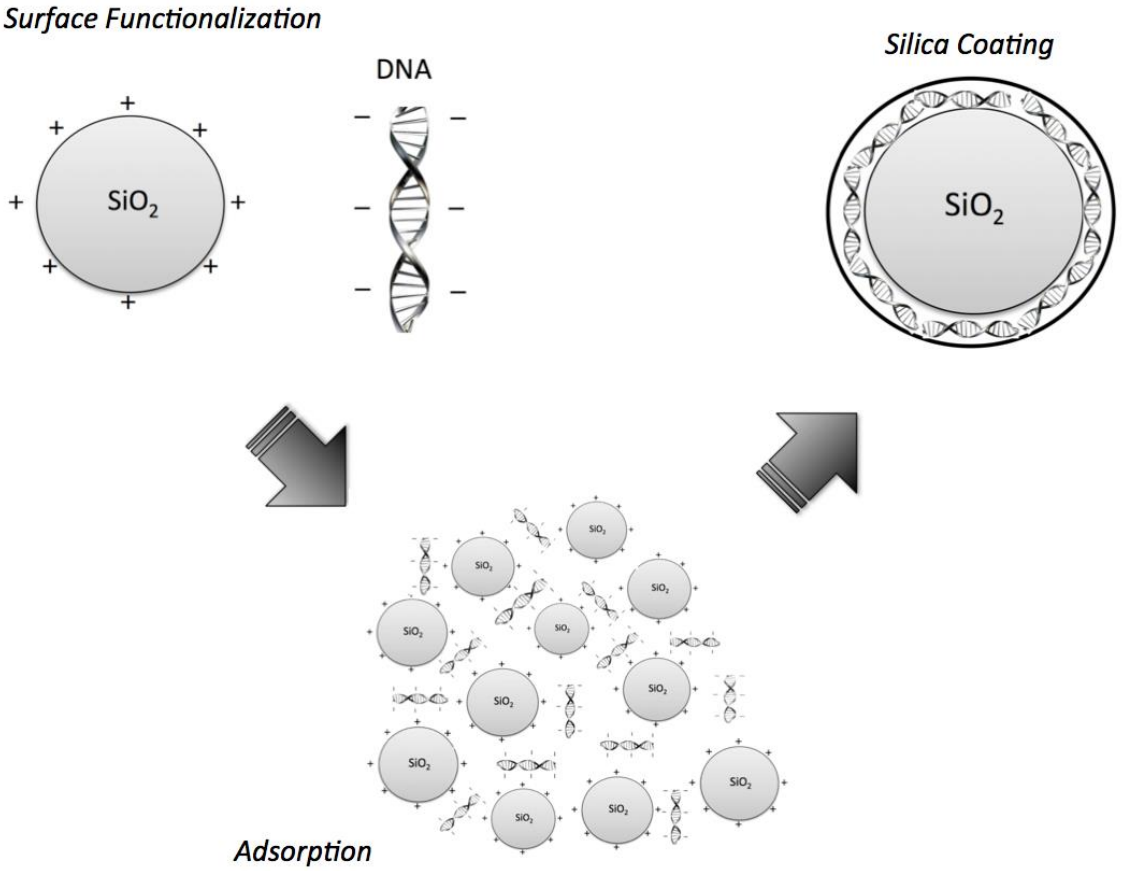

Figure 1-1: Simplified illustration depicting the major processes by which DNA embedded silica nanoparticles are constructed. Synthetic DNA is adsorbed onto charged silica nanoparticles. Silica is then used to coat the exposed DNA and surround the particle. Adapted from Paunescu et al. (2012).

Unlike solid silica nanoparticles, the DNA-encapsulated particles have a tendency to aggregate (Zhang, 2015). This is considered a consequence of the adsorption process, and research is currently underway to develop methods to prevent aggregation.

1.1.1. Silica Complexities

Due to the process pioneered by Paunescu et al. (2012), there is now a means to transport uniquely identifiable information inside nanoparticles at any scale. This process, however, necessitates the use of silica as the seed and shell surrounding the synthetic DNA.

The geothermal community is very familiar with silica, as it often deposits in the form of scale along its route from the reservoir to production. Scaling can have expensive consequences for geothermal operations. Decreased performance of injection wells and turbine damage require routine maintenance in such cases. While some general practices

have been adopted to keep silica from precipitating, much is still not fully understood concerning the complexities of silica deposition and dissolution.

A silica particle tracer is vulnerable to both dissolution and deposition, particularly at the nanoscale. A nanoparticle has a tremendous percentage of its overall volume exposed as surface area, which makes it significantly more vulnerable to interactions with the reservoir fluids, rock matrices and suspension fluid through which it travels.

Dissolution would negatively affect a nanoparticle's ability to carry and protect synthetic DNA. At the same time, silica nanoparticles may act as nucleation sites for mineral precipitation (Brinton et al., 2011). This would cause the particles to increase in size and therefore decrease their chance of traveling through the flow paths of the reservoir.

Two mechanisms of silica precipitation are monomeric and polymeric deposition (Iller, 1979; Brinker and Scherer, 1990). Monomeric deposition is described as the direct deposition of silica molecules onto solid surfaces. Polymeric deposition is the formation of a colloid in solution and its subsequent precipitation. While both depositions are composed of silica, monomeric is a hard, dense deposit and polymeric is a softer, porous silica scale (McLin et al., 2006). With high levels of supersaturation, polymeric deposition is favored. As more and more silica precipitates out of solution, monomeric deposition eventually dominates (McLin et al., 2006).

A connection has been established between silica deposition and pH of the fluid carrying it in solution. Experimentation indicates that the initial rate of silica monomer polymerization is minimized at a pH of 3, increasing in solutions that are more acidic or basic, but particularly in strongly basic solutions (Bohlmann et al., 1976). Similarly, silica solutions of varying pH (5.5, 8) were mixed with varying concentrations of bentonite (0, 0.1, 1ppm) and flowed through glass tubes of quartz sand while monitoring permeability. It was observed that in basic solutions, even small concentrations of bentonite severely lowered permeability. However, an acidic solution with identical bentonite concentration experienced significantly less permeability damage than the basic solution (Tusara et al., 2014).

While these are important considerations, they are certainly not insurmountable or exclusive to silica nanoparticles. Particle tracers can be modified in a way that helps them function in their intended environment. The purpose of this research was to determine how unmodified silica nanoparticles are affected by a simulated geological environment, and to propose potential modifications based upon these results and existing research.

1.1.2. Mobility

The flow characteristics of a wide variety of nanoparticles have been evaluated in fractured and porous media. Investigation of silver nanowires, hematite nanorice, tin-bismuth (Sn-Bi) nanoparticles and silica microspheres indicated that a spherical shape was more conducive to flow (Alaskar et al., 2012).

Particle diameter appears to have an ideal range for flow characteristics within a particular rock matrix; particles smaller than ideal are subjected to diffusion effects, while those larger can be retained by gravitational settling and physical straining (Cumbie and McKay, 1999). Kanj (2013) proposed as an upper limit for direct plugging a size less than 90% of the samples in the microsystem, but recommended $1/7^{th}$ to $1/5^{th}$ the critical pore throat size as an ideal size range to prevent bridging. The pore throats were analyzed from the Arab-D formation in the Ghawar field. This produced an upper limit of 500 nm with 70–100 nm as the size to prevent bridging. Plugging is when a particle is too large to travel through the pore throat, while bridging is a commonly observed effect of multiple particles being pressed together to seal the pore throat. Bridging can be partially mitigated by reducing particle concentration.

Nanoparticles are subjected to multiple forces inside the reservoir, all of which affect their mobility. For a nanoparticle to serve as an effective tracer, it must be designed to travel along the flow paths of the fluid. At the nanoscale, certain forces have a large influence over particle transport that are otherwise insignificant in larger particles. Kanj (2013) identifies dominant small-scale effects as diffusion, stickiness, laminar flow, surface tension, surface area to volume ratio (ρ_{sv}), and electromagnetic forces. Due to a very low Reynolds number (ratio of inertial to viscous forces), nanoparticles are much more susceptible to viscous forces (Kanj, 2013).

Gao, Saiers and Ryan (2006) flowed polystyrene latex microspheres through packed sand and observed significant particle retention on the air-water interface of small bubbles. It was considered that the air-water interface was more effective at trapping the particles than the sand grains when accounting for surface area. A ten-fold increase in flow rate failed to dislodge the particles from the interface.

To a sufficient degree, particles must resist aggregation, dissolution, adherence to rock surfaces, and settling due to gravity (Kanj et al., 2009). Ames (2011) transported silica nanoparticles successfully through a 10m long slim-tube of packed sand. The presence of nanoparticles in the effluent was confirmed visually in the effluent and through DLS and SEM characterization. Alaskar (2013) observed transport of silica nanoparticles through Berea and greywacke sandstone. Alaskar observed in his experiments that spherically shaped particles of a certain size with surface charge similar to that of the flow medium are more likely to be transported with less attenuation within the porous medium.

Reimus (1995) conducted laboratory-scale experiments in fractures, comparing a nonsorbing solute (iodide) to microspheres of diameters 1.0 and 0.3μm. One of 18 experiments injected 300nm diameter silica spheres through a fracture with estimated 89% recovery. Reimus consistently observed an earlier arrival of microspheres in comparison to the iodide in his tracer experiments. He proposed that this was primarily because the microspheres had lower diffusivity than iodide and tended to remain in the high-velocity streamlines near the centerline of the flow channel longer than iodide. As a result of higher diffusivity, the iodide tended to access stagnant or low-velocity regions along the fracture walls. These assumptions allowed Reimus to achieve better agreement between his model predictions and experimental data. He predicted that as the experimental scale increases,

the nondepositing microspheres would provide an increasingly more accurate estimate of mobile fluid residence time in a fractured reservoir, and that matrix diffusion would dominate nonsorbing solute flow behavior. Subramanian et al., (2013) observed 2-5 nm Carbon Dots with polymer hairs travel through columns of glass beads with greater recovery and speed than a KBr chemical tracer.

Experimental research by Ishibashi et al. (2014) indicated that the high velocity streamlines comprise a small percentage of the overall fracture area. Ishibashi et al. (2014) conducted a laboratory flow analysis of granite cores with single tensile fractures. Confining stress varied from 10-30 MPa, with half the samples experiencing a radial shear displacement of 5 mm. Of the eighteen experiments, it was determined that the flow area ranged from 4-22 % of the fracture plane (Ishibashi et al., 2014).

While a nanoparticle may be subjected to a wide variety of forces, its interactions with surfaces require the particle to be extremely close for a detectable impact. Reimus suggested this distance was about 10% of the radius of the particle. Such forces include Van der Waals dispersion forces, electrostatic forces, electronic (Born) repulsion forces, steric forces, chemical bonding forces, and structural or hydration forces (Reimus, 1995). This further highlights the need for a particle tracer to remain in the high velocity streamlines. Figure 1-2 depicts some of the principle forces impacting a nanoparticle flowing through a fracture.

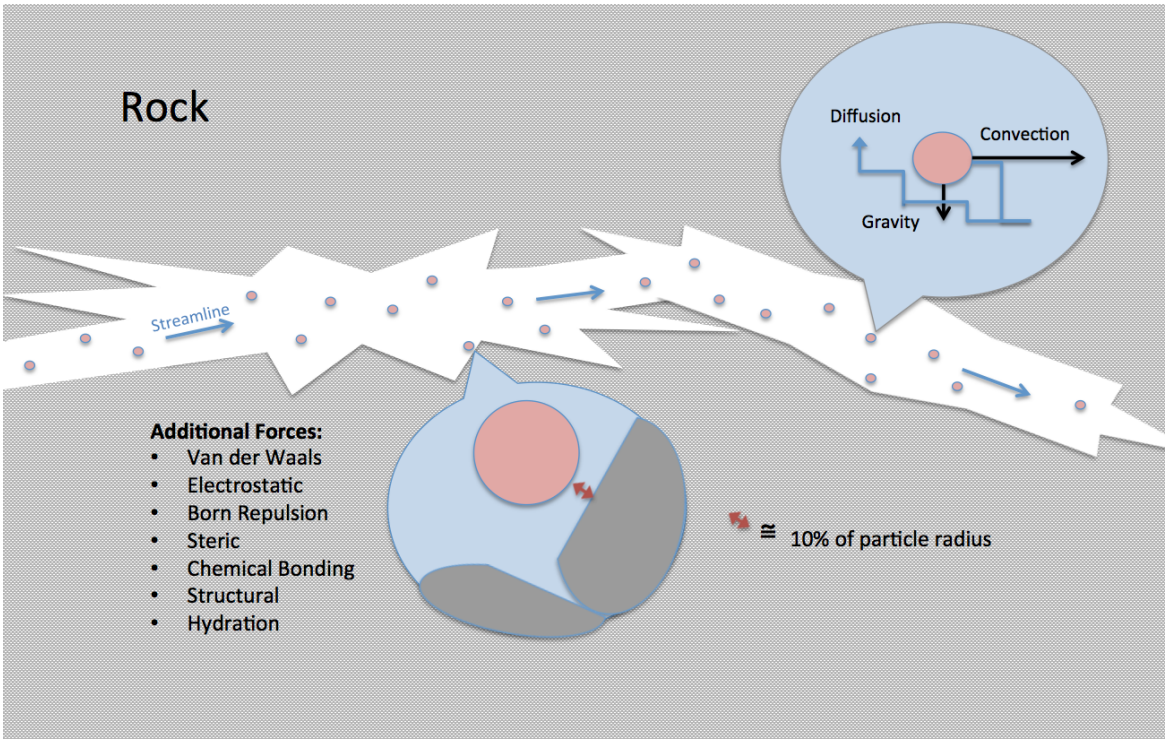

Figure 1-2: Illustration of primary forces governing particle transport through fractures. When particles are very close to the rock surface, forces affecting transport increase substantially. Adapted from Reimus (1995).

1.1.3. Collection and Analysis

Every tracer must have a means of implementation, collection and analysis that is suited to the technical and financial constraints of the operator. One may be inclined to think that anything containing synthetic DNA would extraordinarily expensive. However, a double helix of synthetic DNA can be readily sourced online for reasonable prices. Due to advances in the medical and genetic industries, the process to read the base pairs of a DNA strand is also relatively inexpensive and streamlined. A chemical process called qPCR amplifies the synthetic DNA in order to read its composition (Paunescu et al., 2012). The amplifiable DNA for qPCR detection is extremely low (detection limit ~10^{-6} ng/µl) which is very favorable for tracer applications (Zhang and Manley, 2015).

This report discusses silica nanoparticle heating and injection experiments in separate chapters, followed by a chapter with conclusions and recommendations. Experimental chapters begin with a discussion of prior research, followed by a description of the experimentation for this report and ending with an interpretation and discussion of those results.

Chapter 2

2. Heating Experiments

2.1. Silica Nanoparticles under Heat (Background)

2.1.1. Injection Wells

Decreased performance of geothermal injection wells has resulted in many being studied to better understand contributing processes. One such well is 68-20 in the Coso geothermal field, California. After 5 to 7 years of injecting flashed geothermal fluids, the well was suffering from decreased performance and was redrilled. McLin et al. (2006) performed an analysis of scale deposits from the cuttings samples using SEM imaging and X-ray diffraction. The analysis indicated that loss of injectivity in 68-20 was caused by deposition of silica as opal-A along with trace amounts of calcite near the wellbore (McLin et al., 2006). It was discovered that the injected fluid was supersaturated with silica (up to 940 ppm), which initially deposited as spheres 1-2 μm in diameter. These spheres were found to coalesce over time to form larger spheres up to 10 μm in diameter. Figure 2-1 provides a visual depiction of silica scale from the cuttings of redrilled well 68-20.

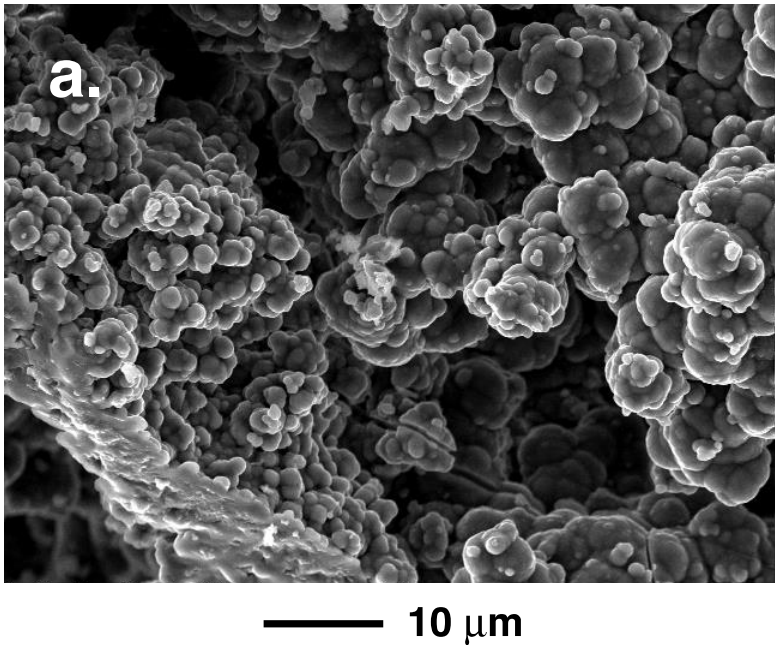

Figure 2-1: SEM image of sample taken from 68-20RD at 869-884m depth. Opal-A spheres 1-2 μm in diameter seen to coalesce to form 10 μm spheres. Reproduced from McLin et al. (2006).

2.1.2. Engineered Geothermal Systems (EGS)

While traditional geothermal reservoirs require heat, permeability and water, a new technology has been developed to exploit low permeability reservoirs of hot, dry rock (Brinton et al., 2011). In most cases such developments utilized hydraulic fracturing, which was previously uncommon in geothermal applications.

Brinton et al. (2011) conducted an evaluation of quartz sand proppants, among other varieties, for use in hydraulic fracturing of geothermal reservoirs. The role of the proppant is to prop open the fractures created in the hydraulic fracturing process, while the rock is still under great pressure from the pumped fluids. Otherwise, after turning off the pumps the fractures would close and subsequently heal. Brinton et al. noted that well suited proppants must not degrade over time or serve as a nucleation site for solid precipitation. Quartz sand proppants were heated in the presence of crushed granite (common EGS target) and three different fluids. The three fluids were deionized water, deionized water spiked with silica using TEOS (tetraethyl orthosilicate) and geothermal water from the Raft River geothermal reservoir (Brinton et al., 2011). Analysis was conducted using SEM imaging and energy dispersive X-ray spectroscopy (EDS). Stainless steel pressure vessels were constructed, and later, quartz glass ampoules, to contain the mixture of fluids, proppants and granite. These vessels were heated to temperatures of 200 to 230°C for periods between 4 and 11 weeks. Unfortunately many of the pressure vessels leaked and the fluid boiled off. However, in the vessels that did not leak, little or no evidence of precipitation was found. Analysis of SEM images indicated that dissolution of quartz sand proppant may have occurred. Brinton et al. attributed this observation to the fact that the geothermal water was undersaturated in silica with respect to quartz at the test temperatures.

2.2. Experimental Apparatus

It was desired to understand the nature of silica nanoparticles under an environment of typical geothermal conditions. The first series of tests was controlled heat experiments at 198°C. This was the maximum sustained temperature of the oil bath.

Pressure vessels were constructed of stainless steel tubing (Sandvik 3R60) with stainless steel end caps. Storage volume for each pressure vessel was estimated at 0.705 mL. Figure 2-2 provides a photograph of a set used for the heating experiments.

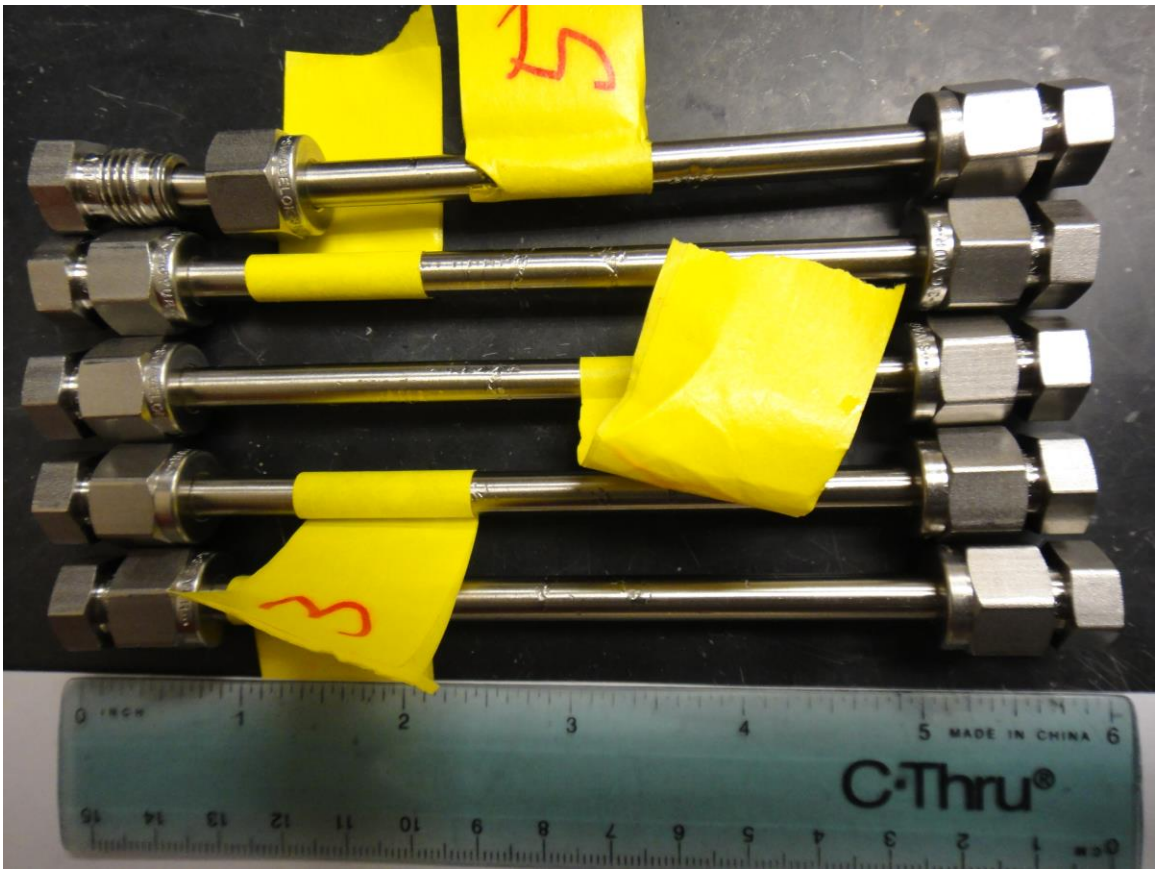

Figure 2-2: Stainless steel pressure vessels used for the controlled heating experiments on solid silica nanoparticles

Five pressure vessels were completely filled with the nanoparticle suspension and sealed. This was to ensure that the fluid inside would self pressurize under the high temperatures and prevent boiling.

An oil bath was heated to 198°C (maximum sustainable temperature) and the five pressure vessels were place inside. At five minute increments, a single pressure vessel was removed. This continued until the last pressure vessel was removed after 25 minutes of heating.

Upon removal from the oil bath, the vessel was placed in a container of room temperature water. The intention was to prevent continued heating of the nanoparticle suspension if the vessel were allowed to cool via air convection. After several minutes the vessel was removed from the water container and tagged with a numbered label.

The pressure vessels were subsequently opened and samples were removed for analysis. Detailed analysis is described for each experiment.

Figure 2-3 depicts the oil bath used for all heating experiments.

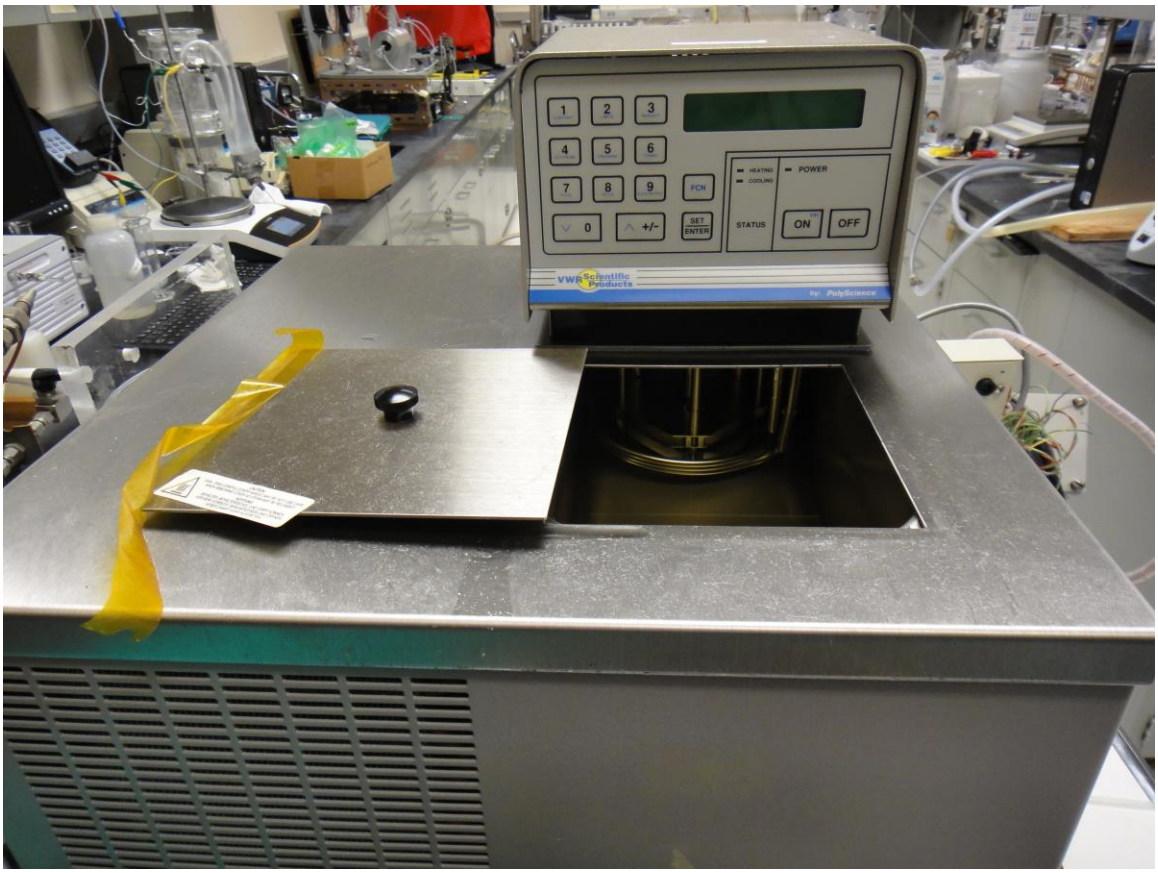

Figure 2-3: Oil bath utilized for the heating experiments. Temperature utilized was 198°C for all experiments.

2.3. 2 μm Diameter Silica SiO_2 Spheres (Test A)

Solid silica particles with 2 μm diameter, suspended in 10 mL water, were purchased for the initial heating experiment. The suspension, provided by microspheres-nanospheres.com (catalog #140214-10) was 5% silica SiO_2. Five pressure vessels were heated at 198°C for varying lengths of time (5, 10, 15, 20, 25 min).

When the pressure vessels were opened for sampling, it was observed that each was still filled with nanoparticle suspension. Samples were pipetted and placed on an SEM stand for image analysis.

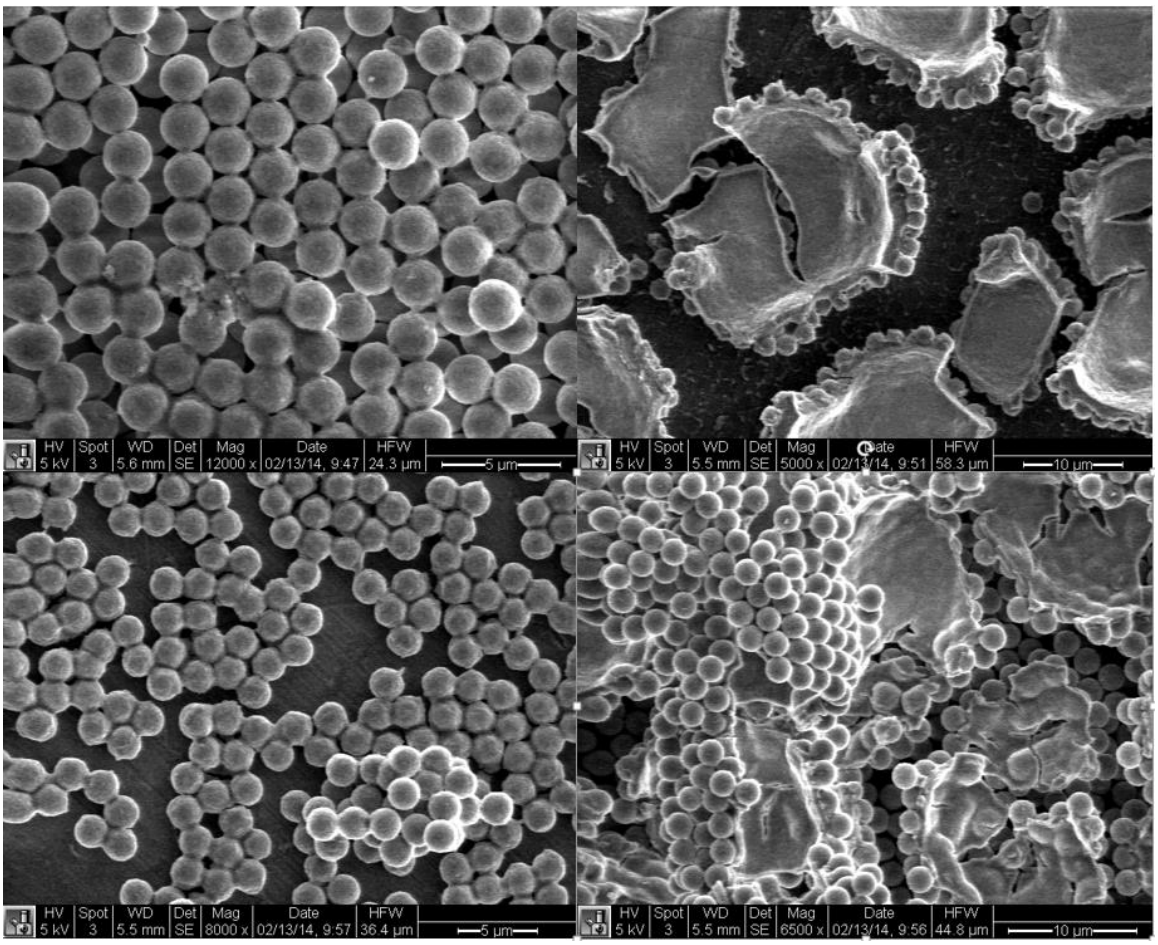

Figure 2-4: SEM images of samples from Test A. Clockwise from top left: 5, 10, 15, 20 minutes. Amorphous silica and coalescence were observed. No significant reduction in particle diameter.

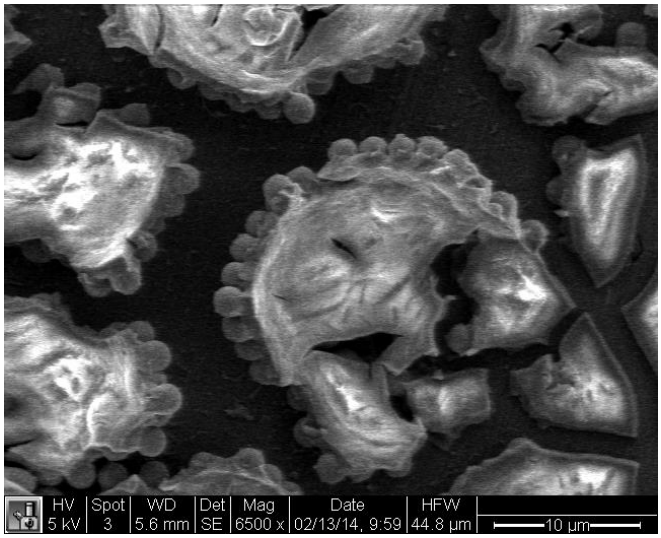

Figure 2-5: SEM image of samples from Test A. 25 minutes heating. Amorphous silica and coalescence were observed. No significant reduction in particle diameter.

Image analysis indicates an abundance of amorphous silica, which appears to have coincided with coalescence of the 2 μm diameter spheres to create larger particles.

2.3.1. Auger Electron Spectroscopy (AES)

It was desired to ensure that all of the precipitate was indeed composed of silica. Upon request, the manufacturer of the stainless steel tubing provided information regarding the temperature limitations of their product. The manufacturer (Sandvik) indicated that 198°C was far below the design limitations of their tubing, and contamination of my nanoparticle suspension by the stainless steel should not be anticipated.

To confirm the absence of contaminants in the nanoparticle suspension, samples were taken from the pressure vessels and configured for analysis under Auger Electron Spectroscopy (AES). Stanford Auger Lab Manager Chuck Hitzman was consulted for the analysis.

Auger Electron Spectroscopy (AES) utilizes a primary electron beam to probe the surface of a solid material. Emitted secondary electrons from the Auger process are analyzed and their kinetic energy is determined. The identity and quantity of the elements are determined from the kinetic energy and intensity of the Auger peaks.

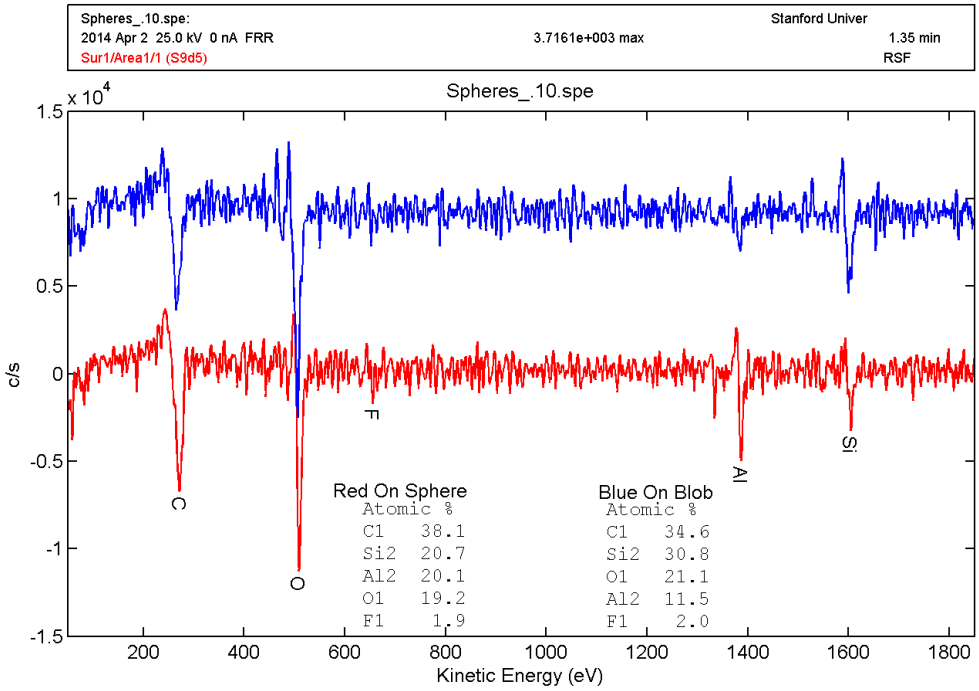

Figure 2-6: Auger Electron Spectroscopy analysis of 2 μm diameter nanoparticle suspension samples following heating at 198°C. Electron beam was focused on the spheres (red) and amorphous silica (blue). Auger characteristic patterns indicate identical compositions.

Figure 2-6 depicts the results of the Auger Electron Spectroscopy. In the analysis, the electron beam was focused separately on the silica spheres and the amorphous silica. Both analyses were plotted on the same chart for comparison. The results indicate an almost identical pattern in Auger peak kinetic energy and intensity. Lab Manager Chuck Hitzman concluded that the two substances demonstrated in Figure 2-5 were indeed of identical composition.

2.3.2. MATLAB Image Analysis

A Matlab code was written to process the SEM images and estimate the true size of the silica spheres in the image. Figure 2-7 shows the 2 μm diameter spheres after 15 minutes of heat exposure.

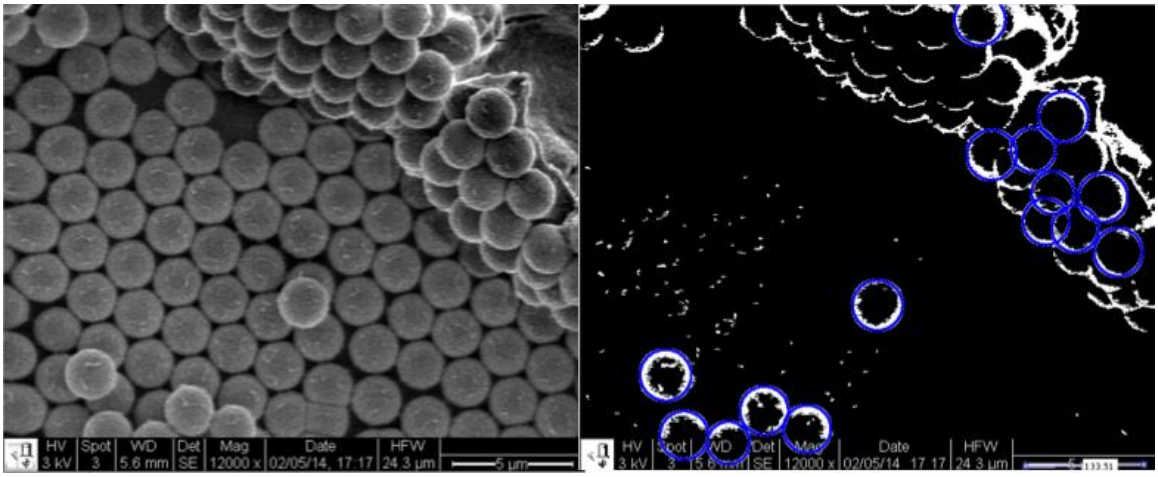

Figure 2-7: SEM image processed and analyzed by Matlab code, showing 2 μm diameter silica spheres after 15 minutes heated at 198°C. Circles were detected, outlined in blue and measured by converting pixels to micrometers.

Fifteen circles were found by the code, and their diameter was calculated by converting pixels to microns using the scale bar in the image. The smallest diameter was 1.769 μm and the largest was 2.141 μm; the average was 1.995 μm. While a certain degree of dissolution and precipitation is evident, integrity of the nanoparticle structure does not appear compromised. In addition, it is likely that the original suspension contained dissolved silica, which would have aided precipitation.

2.4. ~200 nm Diameter Silica SiO_2 Spheres (Test B)

A repeat experiment was conducted to confirm initial findings. The particles used in this experiment were approximately 200 nm diameter solid silica SiO_2 spheres provided by labmate Yuran Zhang. These particles were synthesized at room temperature by the polycondensation of tetraethyl orthosilicate (TEOS) (Zhang and Manley 2015). As a result of this process, the particles were provided in a suspension of ethanol.

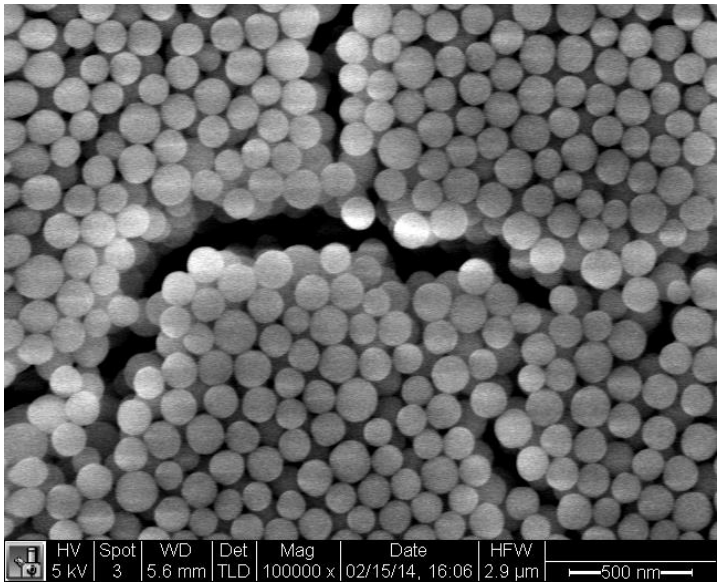

Figure 2-8: SEM image of unheated silica nanoparticle sample used in Test B. Imaging by Yuran Zhang.

The nanoparticle suspension was centrifuged, the supernatant was discharged and ultrapure water was added. This process was repeated several times. The suspension was sonicated until evenly dispersed and pipetted into the pressure vessels.

Five new pressure vessels, identical in design and size, were constructed and heated at 198°C for varying lengths of time (5, 10, 15, 20, 25 min).

When the pressure vessels were opened for sampling, it was observed that each was still filled with nanoparticle suspension. Samples were pipetted and placed on an SEM stand for image analysis.

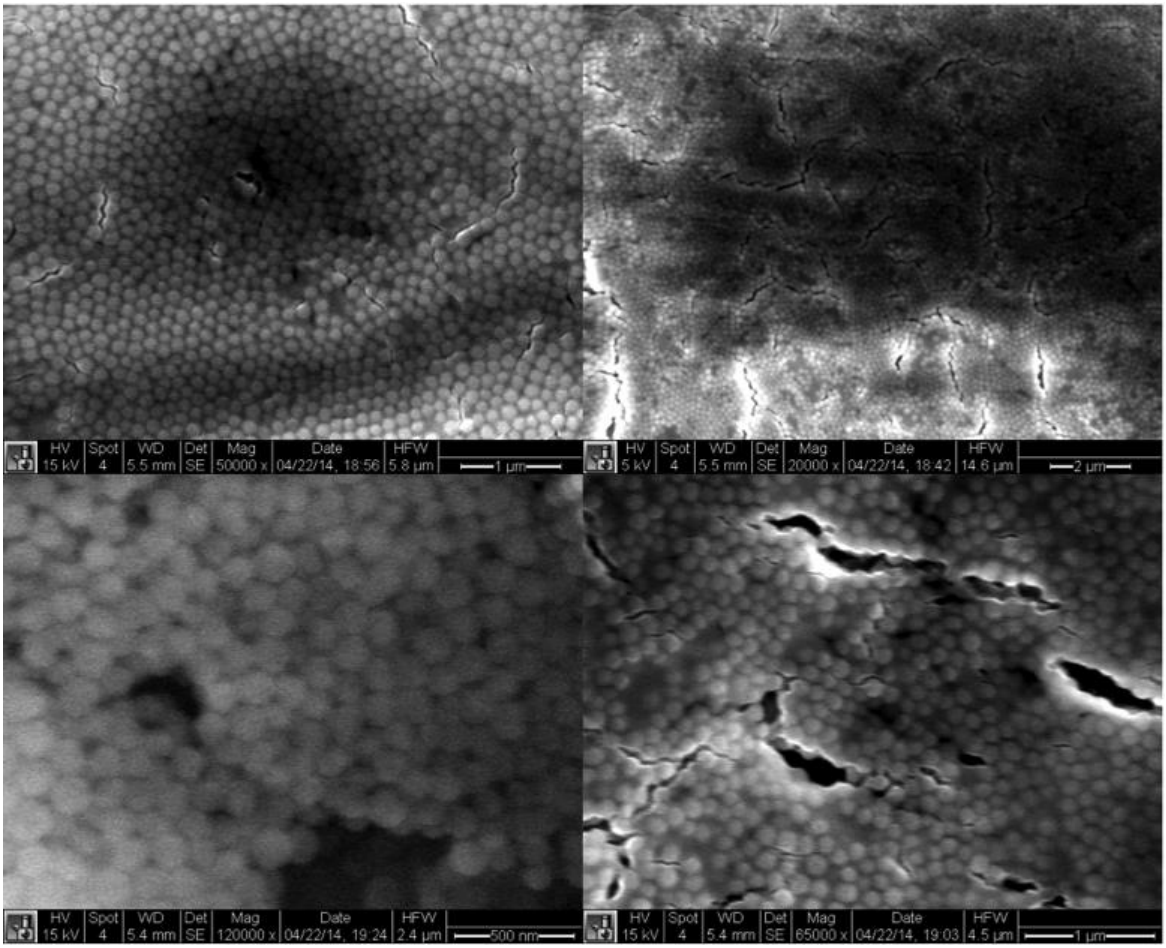

Figure 2-9: SEM images of samples from Test B. Clockwise from top left: 5, 10, 15, 25 minutes. An abundance of amorphous silica was observed along with original spheres.

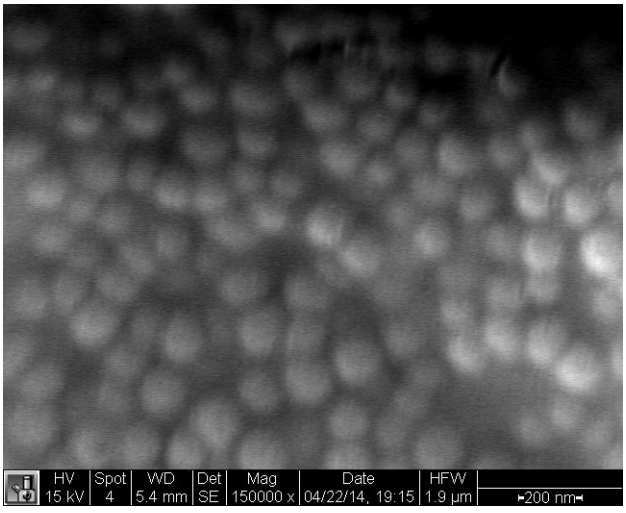

Figure 2-10: SEM image from Test B. Sample heated for 20 minutes at 198°C. Dissolution, amorphous silica deposition and coalescence are evident.

SEM image analysis provided evidence of silica dissolution and subsequent deposition as amorphous silica.

2.4.1. Dynamic Light Scattering (DLS)

This section closely follows the descriptions and explanations of *Zetasizer Nano Series User Manual*. MAN0317 Issue 1.1. Feb. 2004.

Test B samples were further analyzed using Dynamic Light Scattering. The specific device utilized was the Malvern Instruments Zetasizer Nano ZS. Typical applications of dynamic light scattering are the characterization of particles, emulsions or molecules, which have been dispersed or dissolved in a liquid.

Brownian motion is defined as the random motion of small particles in suspension. Motion is caused by the random collision with the liquid molecules that surround the particle[1]. This motion can be measured using a laser light source that penetrates the suspension, is scattered by the particles and collected by detectors at 90 degrees (right angle) or 173 degrees (back angle). Data is typically analyzed at a single angle (Nano ZS uses 173°).

[1] *Zetasizer Nano Series User Manual*. MAN0317 Issue 1.1. Feb. 2004. p 13.2

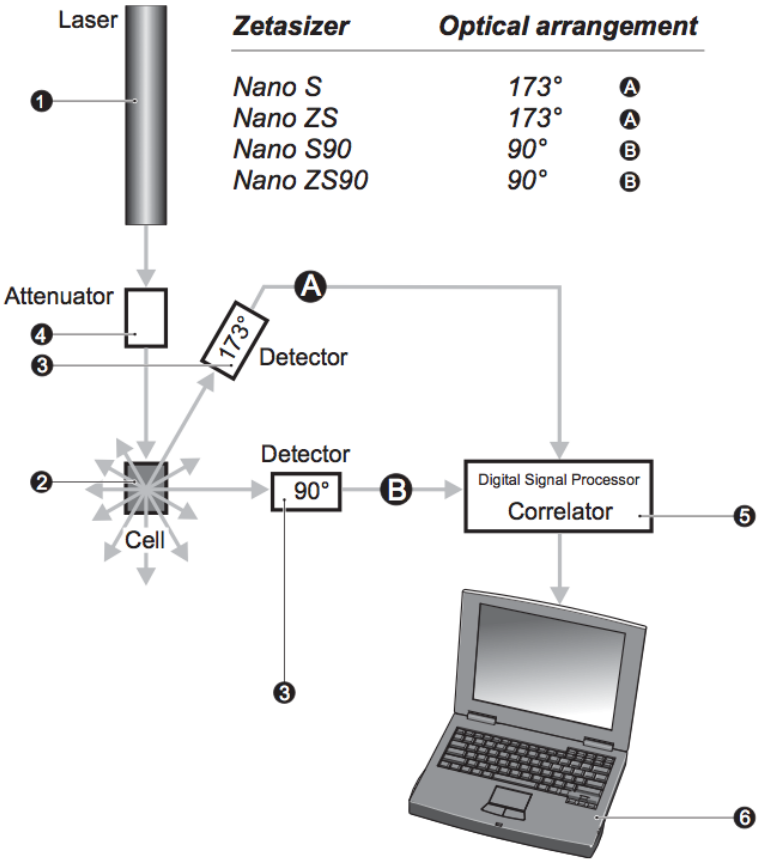

Figure 2-11: Illustration of the DLS apparatus. The attenuator adjusts the laser intensity to optimize the range of the detector. Note that some models use a 90° scattering angle. Reproduced from *Zetasizer Nano Series User Manual* MAN0317 Issue 1.1. Feb. 2004.

The scattered light forms a pattern of dark and bright spots, which grow and diminish in intensity as the particles move in the suspension. DLS monitors the rate of fluctuation in light intensity over a total period of milliseconds and correlates this to the particle size. Large particles have a slower fluctuation in light intensity than small particles. Therefore light intensity fluctuations of smaller particles decay more quickly than large particles.

Devices that utilize backscatter detection (close to 180°) have some advantages over other angles of detection. One of the greatest challenges for DLS is caused by multiple scattering, or light being scattered by more than one particle. Backscatter detection does not require the incident beam to penetrate the entire sample, thereby allowing higher sample concentrations without data contamination.

With the knowledge of the suspension fluid's refractive index and viscosity, the measurements results can be interpreted. The correlator interprets the optical data and relates the decay to particle size. A monodisperse suspension, in which the particles are uniform in size, follows a decay of the form:

$$\boldsymbol{G(\tau) = A[1 + B\exp(-2\Gamma\tau)]}$$

1

where:

- A = baseline of the correlation function
- B = intercept of the correlation function
- Γ = decay constant
- τ = time delay

The diffusion coefficient D_t is calculated using

$$\boldsymbol{\Gamma = D_t q^2}$$

2

where

$$\boldsymbol{q = \frac{4\pi n}{\lambda} \sin\left(\frac{\theta}{2}\right)}$$

3

and

- n = liquid refractive index
- λ = wavelength of laser light
- θ = scattering angle
- q = scattering vector

For a suspension of polydisperse particle sizes, the decay function can be expressed as:

$$\boldsymbol{G(\tau) = A[1 + B\, g_1(\tau)^2]}$$

4

where $g_1(\tau)$ is the sum of all exponential decays in the correlation function.

The Stokes-Einstein equation incorporates a diffusion coefficient from the DLS data along with suspension fluid properties to calculate hydrodynamic diameter of the particles.

$$\boldsymbol{D_h = \frac{k_B T}{3\pi\eta D_t}}$$

5

where:

- D_h = hydrodynamic diameter
- D_t = translational diffusion coefficient
- k_B = Boltzmann's constant
- T = thermodynamic temperature
- η = dynamic viscosity

This relationship reveals the critical importance of temperature in both T and η.

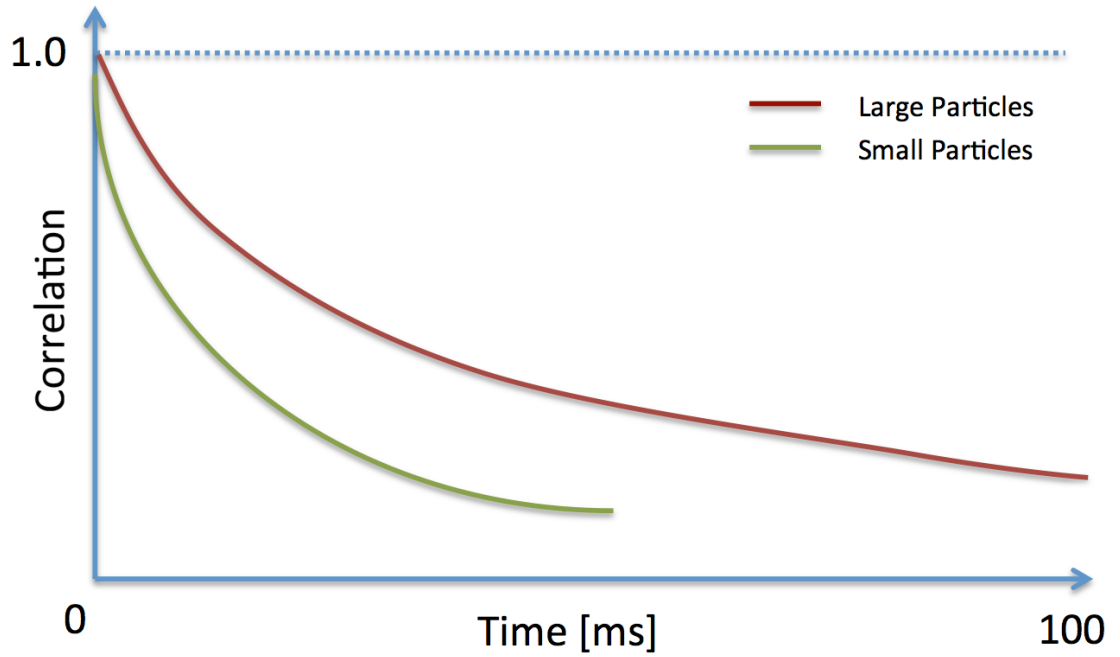

Figure 2-12: Illustration depicting the difference in decay rates between large and small particles. Large particles diffuse more slowly and therefore maintain correlation longer. Note that the time scale is typically on the order of tens of milliseconds[2]. Adapted from *Zetasizer Nano Series User Manual*. MAN0317 Issue 1.1. Feb. 2004.

Another critical assumption is that the particles undergoing Brownian motion are spherical. D_h provides the diameter of spheres that would diffuse in the same way as the particles being analyzed.

It is important to note that the hydrodynamic diameter D_h is calculated with the assumption of smooth spherical particles in the absence of ionic forces. A rough surface would reduce the diffusion speed, thereby artificially increasing the hydrodynamic diameter[3]. In a low-conductivity medium with the presence of ions, an electric double layer called the Debye length (K^{-1})[4] could develop and reduce the diffusion speed. The addition of 10 mM NaCl appears to increase the conductivity and suppress the electrical double layer, allowing an accurate measurement.[5] Of course, a nonspherical particle would not diffuse in the same way as a spherical particle of comparable size. Therefore, detailed attention must be applied to the characteristics of the measured particles.

[2] *Zetasizer Nano Series User Manual*. MAN0317 Issue 1.1. Feb. 2004. p 13.3.

[3] "Dynamic Light Scattering: An Introduction in 30 Minutes." DLS technical note MRK656-01. Malvern Instruments.

[4] "Dynamic Light Scattering: An Introduction in 30 Minutes." DLS technical note MRK656-01. Malvern Instruments.

[5] "Dynamic Light Scattering: An Introduction in 30 Minutes." DLS technical note MRK656-01. Malvern Instruments.

While DLS is an exceptional tool for measuring nanoparticles in suspension, there are some inherent assumptions in its calculations. Agglomerated, nonspherical particles are less accurately predicted. With particles of greater size distribution, the z-average size provided by DLS is less accurate.

This ends the material derived from *Zetasizer Nano Series User Manual*. MAN0317 Issue 1.1. Feb. 2004.

2.4.1.1. Dynamic Light Scattering Results

A sample was pipetted from each of the five pressure vessels of Test B and placed in separate cartridges for DLS analysis. An additional unheated sample of the identical suspension was analyzed using DLS. In order to meet the requirements of DLS, each sample was heavily diluted. A few drops of the sample would be diluted to a few mL of suspension with distilled water.

The DLS software produces data and plots a graph of the size distribution. The size distribution plot of the unheated results are shown in Figure 2-13.

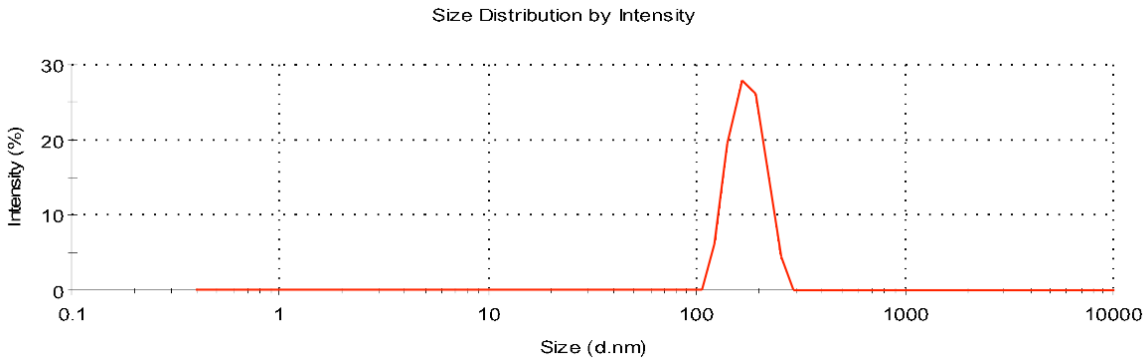

Figure 2-13: DLS size distribution plot for unheated nanoparticle suspension. Analysis concluded a z-average of 175.1 nm. The single peak and relative monodispersion increases confidence in this value[6].

A z-average value was provided for each sample. The values are depicted in Table 1. The average particle diameter showed an initial decrease until approximately 20 minutes of heating, at which point size dramatically increased. This confirms the notion of dissolution followed by amorphous silica deposition and coalescence.

[6] *Zetasizer Nano Series User Manual*. MAN0317 Issue 1.1. Feb. 2004. p 5.6.

Table 1: DLS Results (Test B)

Sample	Unheated	1	2	3	4	5
z-average diameter (nm)	175.1	158.2	160.1	155.2	2238	1650

2.5. Interpretation and Discussion

It must be noted that the ratio of silica mass to water was not identical in the two tests. Another important observation is that the two sets of particles are drastically different in size (2000 nm vs 200 nm). As a particle decreases in size, the percentage of mass on its surface increases. Therefore, a greater percentage of the particle's mass is subject to interactions with surrounding fluids, rock matrices, etc. For this reason one would expect a small particle to be more chemically reactive than an identical particle of larger size.

At any rate, both dissolution and amorphous deposition was observed in both tests. The tests were static and the heated pressure vessels were quenched in room temperature water. It is likely most of the amorphous silica was in solution until the rapid temperature reduction, which caused it to precipitate out.

In both tests, particle integrity was maintained. Dissolution appeared generally uniform amongst the particles viewed under SEM. While the smaller nanoparticles saw more diameter reduction than the larger particles, the degree of dissolution was not deemed severe. Deionized water was used as the suspension fluid in both tests, which is known to be more chemically aggressive than that of geothermal fluids (Brinton et al., 2011).

Patterns of dissolution and precipitation were consistent with observed silica scale in the redrilled injection well 68-20 at the Coso geothermal field, California. Smaller spherical nanoparticles coalesced to form larger particles. Amorphous deposition had a smooth appearance and appeared to bind together many spherical nanoparticles.

Dynamic Light Scattering analysis on samples from Test B depicted a trend of decreasing nanoparticle diameter followed by a drastic increase in diameter after 20 minutes exposure to heat. While the trend is certainly accurate, the exact value of z-average must be recognized as a relation to spherical particles. Coalesced silica particles will not undergo Brownian motion in the same manner as a sphere. The results appear to support initial dissolution followed by precipitation of amorphous silica and coalescence.

Chapter 3

3. Injection Experiments

Silica nanoparticles were injected through a tube of packed sand at temperatures of 25°C, 120°C, and 150°C.

3.1. Injection of Nanoparticles (Background)

Past experiments, described in this section, have demonstrated the ability to inject silica nanoparticles through porous media and retrieve them in the effluent.

Ames (2011) injected SiO_2 (silica) nanoparticles successfully through a 10 m long stainless steel slim tube filled with packed sand at room temperature. The spherical particles were relatively monodisperse with a modal diameter of 350 nm (Ames, 2011). A total of 10mL of nanoparticle suspension was injected (approximately 20% of 1 pore volume). Effluent samples were collected periodically and characterized with Dynamic Light Scattering and SEM image analysis. The silica nanoparticles were visually detected as a cloudy white powder in the effluent following the injection of approximately 0.5 pore volumes of water. After 2 pore volumes injected, nanoparticles were still present but no longer at high enough concentration for visual detection. Permeability was monitored throughout the experiment. It fluctuated slightly but remained relatively constant around 50 ± 4 darcy (Ames, 2011).

Alaskar (2013) demonstrated successful transport of solid SiO_2 (silica) nanoparticles through Berea sandstone. An attempt to inject an assortment of silica nanoparticles through low permeability greywacke sandstone had inconclusive results.

For the Berea sandstone injection, negatively charged spherical silica nanoparticles with an average diameter of 100 nm were flowed through a core and detected in the effluent. According to Alaskar (2013), filtration theory predicted that the probability of SiO_2 transport by diffusion, interception and gravity settling was low for this experiment. Gravity and interception were negated because the particles were small with a density similar to the suspension fluid. Straining was considered unlikely because the average pore throat of the Berea sandstone, determined by mercury intrusion method, was 8.8 μm (88 times larger than the average silica particle diameter). Effluent samples were analyzed using Dynamic Light Scattering and SEM image analysis. The 100 nm silica nanoparticles were easily identified from rock fines, as illustrated in Figure 3-1. The Berea sandstone core was subsequently cut. Spherical silica nanoparticles were detected in slices from the center of the core, demonstrating that they accessed the pore spaces.

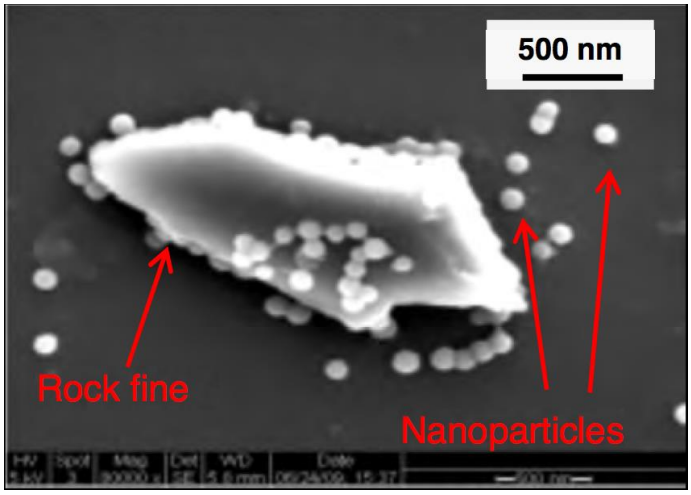

Figure 3-1: Alaskar illustrates the ease in detecting 100 nm silica nanoparticles amongst Berea sandstone fines. The particles were successfully injected and detected in the effluent. Reproduced from Alaskar (2013).

For the greywacke sandstone injection, a mixture of three different sizes of silica nanoparticles was used in the suspension. 1, 0.3 and 0.2 mL of 70, 200 and 350 nm nanoparticles respectively were mixed and injected. The pores of greywacke were measured with mercury intrusion and found to be an average of 60 nm and maximum of 150 nm. With the average pore size smaller than the smallest nanoparticle used, straining was a major factor in filtration. The results were inconclusive because particles larger than 150 nm were detected in the effluent. It was speculated that the particles might have slipped through the space between the core wall and the core-holder rubber sleeve due to insufficient confining pressure (1000 psig). Slices of the core were made, but SiO_2 nanoparticles were not visible under SEM image analysis. Some of the effluent resembled broken silica nanoparticle spheres, and it was suspected that some nanoparticles may have been crushed. A subsequent pressure test was conducted outside the core at pressures up to 2000 psig, but the silica nanoparticles did not exhibit any distortion or damage. The injection pressure was 700 psig.

Alaskar (2013) also injected DNA-embedded silica nanoparticles obtained from Daniela Paunescu, Institute for Chemical and Bioengineering at Eidgenoissische Technische Hochschule Zurich. The mean particle size was approximated at 175 nm using SEM and TEM (Transmission Electron Microscope) image analysis. It was also determined that the outer silica layer, which protected the DNA, comprised 10-12.5 nm of the 175 nm diameter. A nanoparticle slug was injected via syringe into the apparatus and flowed through a stainless steel tube filled with packed Ottawa sand. Flow through the apparatus was constant at 1 mL/min, and approximately 2 mL of nanoparticle suspension was injected (20% of the pore volume). The injection experiments were conducted at 25°C and elevated temperatures of 120, 150 and 180°C. In order to prevent boiling, a system pressure of 4, 7 and 12 atm respectively was maintained using a back-pressure regulator. Constant mass flow rate was monitored using a mass balance and stopwatch.

Effluent from the injection experiments was sampled and subsequently analyzed by Alaskar (2013) using electron micrograph imaging. At room temperature, neither particle size reduction nor aggregation was observed. As the temperature increased to 150°C, the particle size was reduced by an approximate factor of four. Aggregation was also observed in the injection experiments at elevated temperatures.

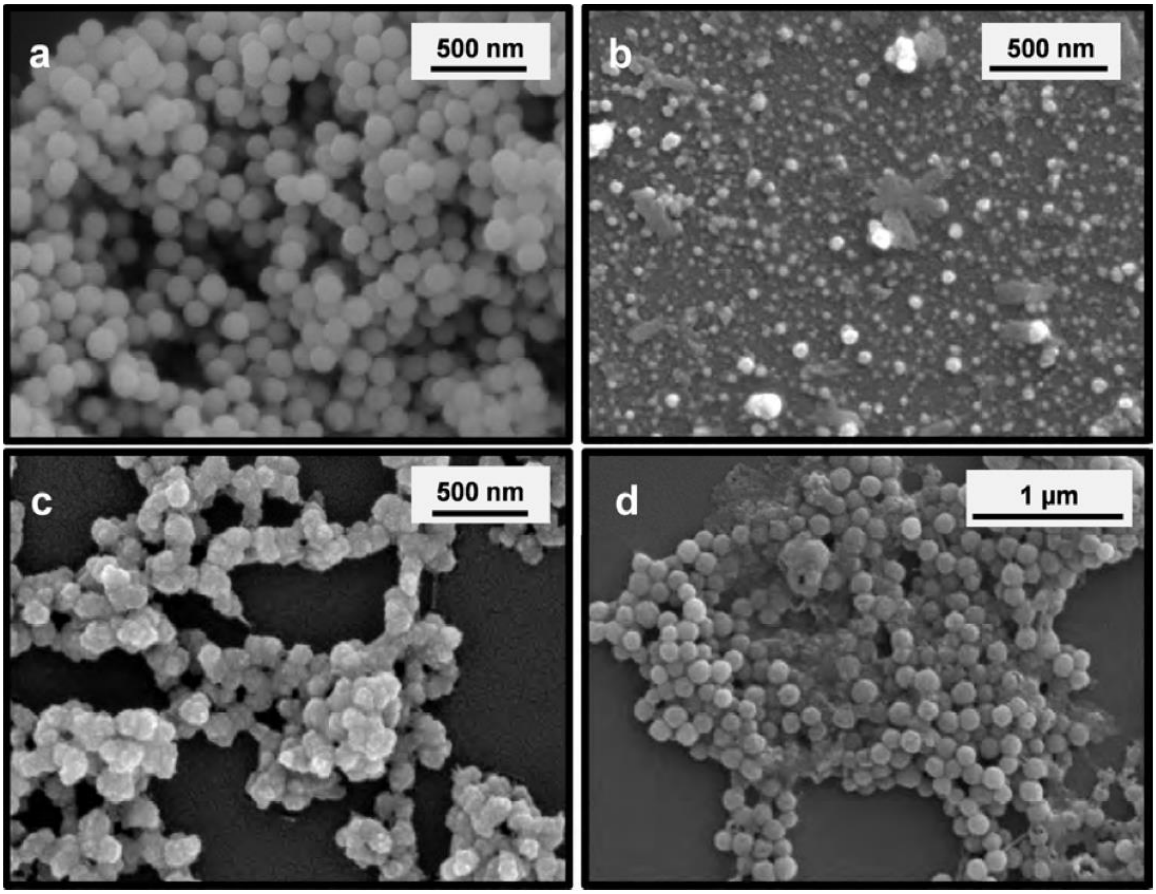

Figure 3-2: Electron micrograph images from Alaskar (2013) injection of DNA embedded silica nanoparticles. For 150°C injection, (a) depicts the influent, while (b) and (c) depict the effluent. (d) displays effluent from the 25°C injection. Note that the room temperature experiment did not result in particle aggregation or size reduction. Reproduced from Alaskar (2013).

Alaskar (2013) concluded that the shape, size and/or size distribution and surface charge of the particles were influential parameters governing the transport of nanoparticles through porous media. Spherical shapes were demonstrated to flow more easily. In an experiment involving hematite nanorice, coating the particles with a surfactant increased the recovery from zero to 23% (Alaskar, 2013).

Tusara et al. (2014) conducted injection experiments through packed quartz sand at 80°C with pH values of 5.5 (acidic) and 8 (basic). The injected fluid was composed of a synthetic silica solution of 700 ppm and a bentonite suspension of 0, 0.1 and 1 ppm concentration.

The solubility of silica at 80°C was determined to be slightly less than 300 ppm. Bentonite is a material often used for mud in drilling operations, as well as a clay that occurs commonly in nature. The porous column was composed of five 5 cm glass tubes with a diameter of 0.4 cm connected in series and filled with packed sand. The glass tubes were placed in a water bath at 80°C for the duration of the experiments. Permeability calculations were made, and data was plotted as a ratio to the baseline permeability against time.

In both acidic and basic experiments, an increase in bentonite concentration accelerated the loss of permeability. In basic experiments, this loss of permeability occurred more quickly. Total and monomeric silica concentrations were monitored in the effluent and compared to the influent. In the experiment with pH 8 and 1 ppm bentonite, the concentration of both total and monomeric silica concentrations dropped significantly. This run also contained the most severe drop in permeability. Tusara et al. (2014) suggested that two primary deposition mechanisms were contributing to the permeability loss: the deposition of monomeric silica onto the quartz sand grains and independently from that, onto the suspended material.

3.2. Experimental Apparatus

The apparatus was designed to push fluid through packed sand inside a heated air bath, cool the fluid, and then discharge the effluent at a sampling point. Connected via a network of stainless steel tubing were the following components:

- Eldex pump (max operating pressure 6000 psi, flow rates 0.01 to 10 mL/min)
- Air bath (max operating temperature 400°C)
- Enlarged stainless steel tube containing packed Ottawa sand
- Mechanical differential pressure gauge (5 psi scale. 0.2 psi increments)
- Standard pressure gauge (100 psi scale)
- Back pressure regulator
- Water pocket (room temperature)
- Mass balance
- Thermocouple

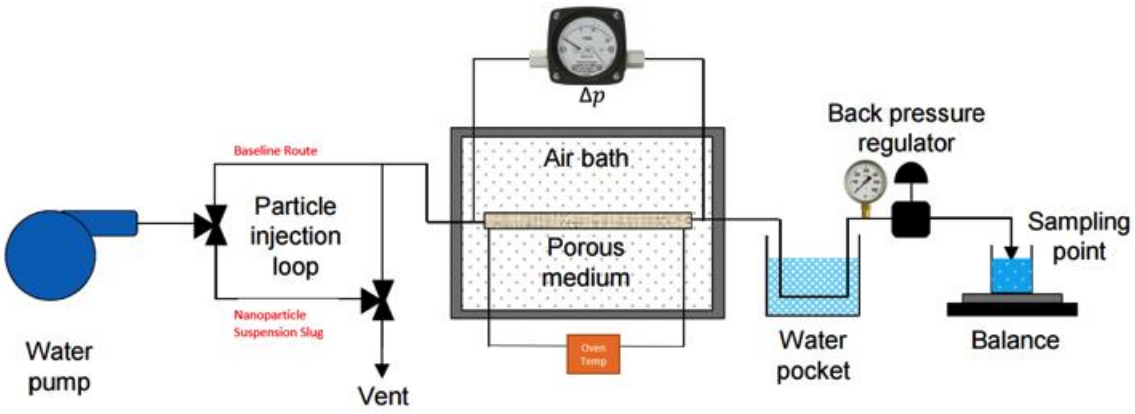

Figure 3-3: Injection experiment apparatus. The air bath temperature was confirmed using a thermocouple. System pressure was monitored as well as differential pressure. Adapted from Alaskar (2013).

After each experiment (except 6), the sand pack was removed and the stainless steel tube was flushed with deionized water. Fresh sand was packed into the enlarged tube and retained by a stainless steel mesh. The enlarged tube was reinstalled into the apparatus.

An effort was made to evacuate air from the apparatus prior to experimentation. Shop vacuum was applied to the apparatus through a fitting downstream of the water pocket. After a period of time under vacuum, a three-way valve was turned which opened a bypass route around the water pump. Deionized water was observed flowing through this clear plastic bypass route. After a couple minutes, a steady stream of deionized water was observed exiting the vacuum fitting and the vacuum fitting was closed. The three-way valve was turned to seal off the bypass route and reactivate the original route. The water pump was started, and eventually water was observed exiting as effluent at the sampling point. When this flow was steady, the sampling point was sealed with a valve, and the seals were loosed which connected to the differential pressure gauge. When steady flow was observed leaving these seals, both were securely tightened.

The nanoparticle slug was stored within a section of stainless steel tubing, which was accessed by turning a three-way valve to redirect flow from the water pump through the slug section. The redirected water flow pushed the slug through the network of tubing and into the sand pack. The same slug volume was used in each experiment. Using measurements of the inner diameter and length of the section of tubing used, the slug volume was estimated as 1.5 mL (approximately 15% pore volume). The nanoparticle slug was installed into the apparatus as late as possible in order to avoid gravitational settling. It is estimated that the slug was installed 5-15 minutes prior to the time at which the three-way valve was turned for injection into the sand pack. The section of stainless steel tubing containing the slug was filled using a pipette. The nanoparticle suspension was first sonicated to ensure adequate dispersion of the particles in the suspension. The section of tubing containing the slug was thoroughly flushed with deionized water and blown dry with pressurized air. The slug suspension was then pipetted through one end of the tubing

until a steady stream was observed leaving the opposite end. The two ends of the tubing were then attached to the apparatus using stainless steel screw fittings.

For each experiment, the air bath was heated to the prescribed temperature. This was confirmed with a thermocouple mounted inside the air bath.

Figure 3-4: Air bath used for injection experiments. Note the thermocouple on the right, and the enlarged stainless steel tube on the left which contains the sand pack.

The Eldex pump was set to a prescribed flow rate (typically 2.50 mL/min) throughout the experiment. The pump is designed to maintain flow rate regardless of pressure. A steady mass flow rate was confirmed using the mass balance to measure effluent as a function of time. It was observed that by adjusting the back-pressure regulator to maintain steady system pressure, the mass flow rate would stabilize.

System pressure was measured using a standard fluid pressure gauge. Steam tables were consulted for acceptable pressures to prevent boiling of water inside the air bath. The system was not pressurized for experiments at room temperature. For experiments at 120°C, the system pressure was 32 psi (2.2 atm); for 150°C it was 90 psi (6.1 atm).

Differential pressure was measured via stainless steel tubing conduits that were connected to the inlet and outlet of the sand pack using a T-fitting on the primary flow line. These pressure lines were routed from the sand pack, through an instrument port in the air bath and terminated at the differential pressure gauge. The differential pressure gauge was equipped with a fitting for both inlet and outlet pressure lines.

Data collected during the experiments were differential pressure readings, effluent samples and sampling times. The "baseline" differential pressure reading was considered to be the value representative of pure deionized water, at the prescribed temperature, flowing through the sand pack. The baseline point was considered established when steady flow had commenced, system pressure was maintained, the air bath was at the prescribed value, and the differential pressure had stabilized for several minutes. As the injected fluid was heated to its prescribed temperature, the fluid viscosity would decrease and therefore the differential pressure. This value would then stabilize as the fluid temperature stabilized. When the baseline point was reached, the three-way valve was turned to inject the nanoparticle slug and the clock was started. Differential pressure values were recorded at one-minute intervals. Effluent samples were taken roughly every two minutes, beginning 3.5 - 5 minutes after the valve was turned. The experiments ran for 30 minutes.

Permeability, k [darcy] was calculated using Darcy's Law.

$$\boldsymbol{k = \left(\frac{Q}{A}\right)\mu\frac{L}{\Delta p}} \qquad \textbf{6}$$

where

- Q = flow rate [mL/s]
- A = cross sectional area of the porous column [cm^2]
- μ = viscosity [cp]
- L = length of the porous column [cm]
- Δp = pressure drop across the porous column [atm]

3.3. Solid Silica Nanoparticle Injection Experiments

The solid spherical nanoparticles used in the injection experiments were synthesized by labmate Yuran Zhang. All injection experiments of solid silica nanoparticles utilized the same batch. The nanoparticle suspension was delivered as 2 mL washed silica nanoparticles "ss2". The particles were suspended in ethanol, without residual reagent. The nanoparticle suspension was subsequently centrifuged multiple times, pouring off the supernatant and adding ultrapure H_2O each time. Prior to experimentation the nanoparticle suspension was sonicated to ensure adequate dispersion.

The particles were spherical in shape with an average diameter of approximately 200 nm.

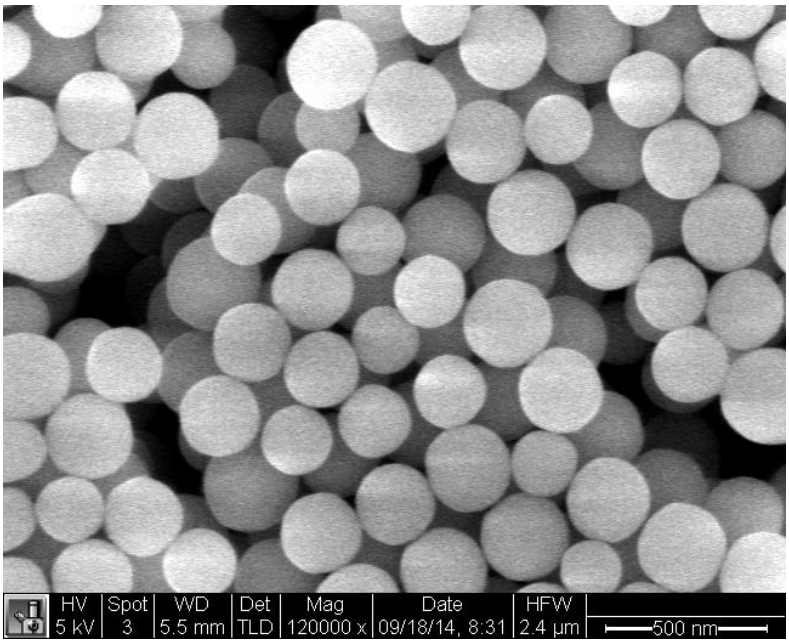

Figure 3-5: SEM imaging of the ss2 solid silica nanoparticles prior to injection experiments. Note the spherical shape and that they are relatively monodisperse in size. Imaging by Yuran Zhang.

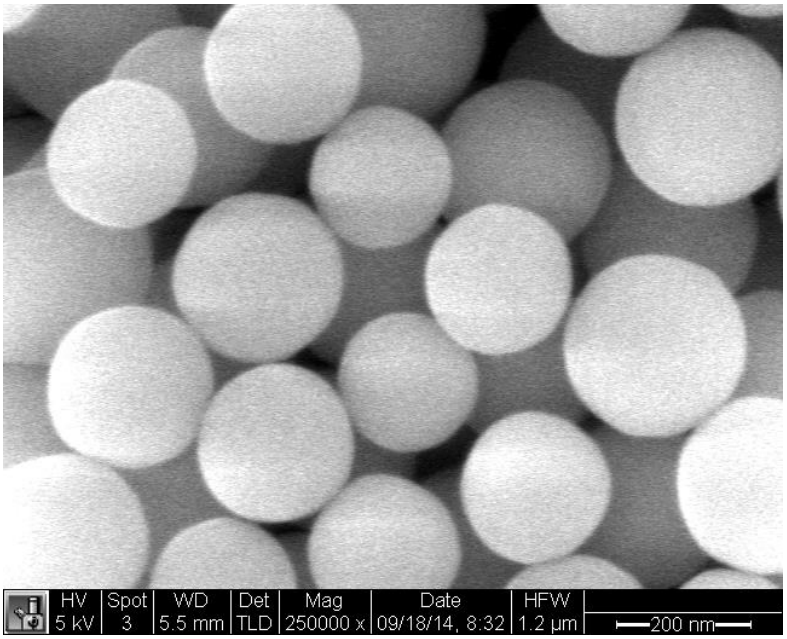

Figure 3-6: SEM imaging of the ss2 solid silica nanoparticles prior to injection experiments. Illustrates an approximate average diameter of 200 nm. Imaging by Yuran Zhang.

Injection experiments of solid silica nanoparticles were divided into three groups, based primarily on the residence time inside the packed sand along with other small differences. Experiments 1-3 had no residence period, experiments 4-5 had a 1 hour residence period, and experiments 6-7 had a 6 hour residence period.

3.3.1. Injection without residence period (Experiments 1-3)

The first injection experiments were designed to study the transport of silica nanoparticles through porous media, as well as the effect of temperature on particle integrity.

The first experiment was conducted at room temperature. This was the only experiment in which two independent pressure gauges were used to measure the differential pressure. Both gauges were digital, and the inlet pressure was simply subtracted from the outlet. Subsequently a more sensitive differential pressure gauge was implemented, as the elevated temperatures significantly reduce observed differential pressure due to the lowered water viscosity.

This was also the only experiment where the flow rate was not 2.50 mL/min. In experiment 1 the flow rate was 1.20 mL/min. The flow rate was later increased to better observe the differential pressure at elevated temperatures.

Experiment 1 was carried out longer than all the other experiments. Data were collected continuously for 86 minutes. Later experiments were shortened to 30 minutes.

The baseline permeability of the sand pack was determined as 54 darcy. Effluent samples were not taken, as there was no stress of elevated temperature. The effluent was measured to have a pH of 8.

At room temperature, the differential pressure showed a steady rise which leveled off after 10 minutes and remained constant for the duration of the experiment. A 9% drop in permeability was observed as a result of silica nanoparticle injection.

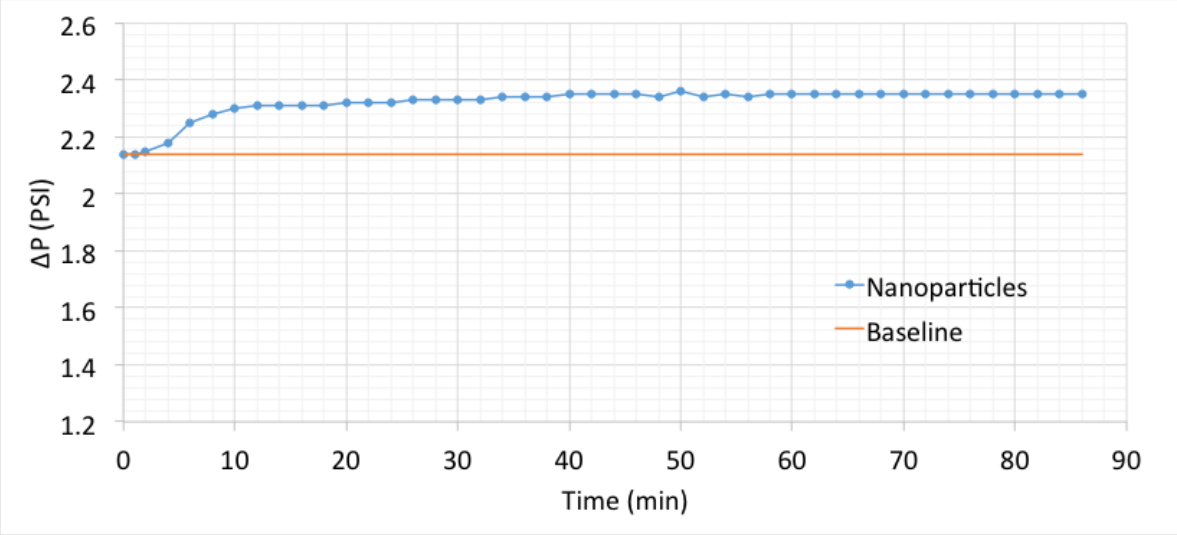

Figure 3-7: Experiment 1 plot of differential pressure vs. time. The orange line is the baseline differential pressure for water only, and was drawn for illustration purposes. The blue line represents measurements of differential pressure after silica nanoparticle injection.

Experiment 2 was conducted at a temperature of 120°C and a flow rate of 2.50 mL/min. Sand pack baseline permeability was determined to be 93 darcy. The effluent was measured to have a pH of 7. Effluent samples were taken periodically and evaluated using SEM image analysis. A different trend was observed compared to experiment 1. The differential pressure rose sharply and then began a decline. The stabilized permeability after nanoparticle injection was calculated to be 86 darcy, an 8% decrease.

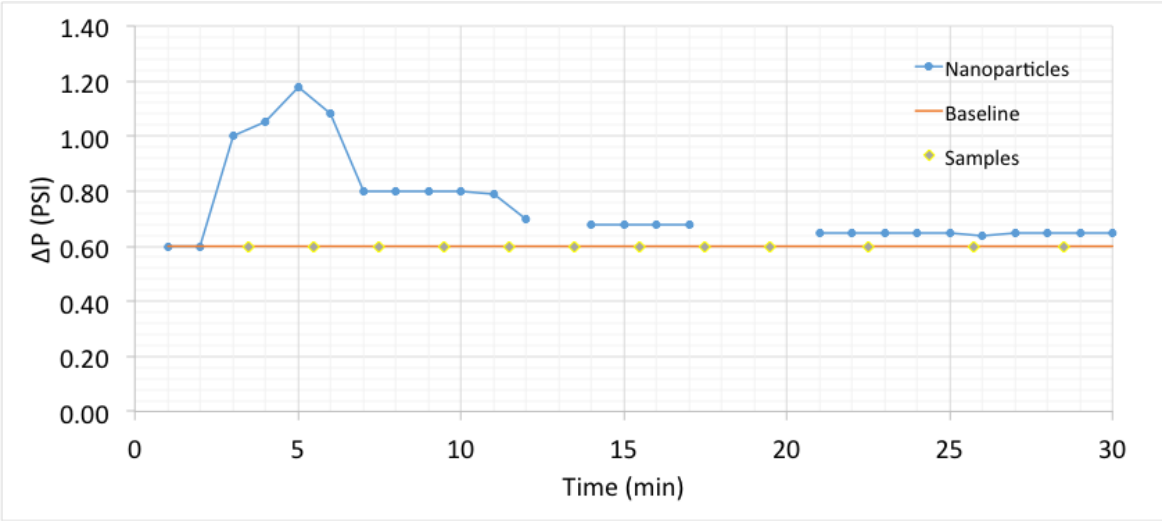

Figure 3-8: Experiment 2 plot of differential pressure vs time. The orange line is the baseline differential pressure for water only, and was drawn for illustration purposes. The blue line represents measurements of differential pressure after silica nanoparticle injection. Sampling times are marked by golden diamonds.

The injected nanoparticles were visible in the second effluent sample (taken 5.5 minutes after slug injection). The spherical shape was maintained and the size appeared consistent with the influent.

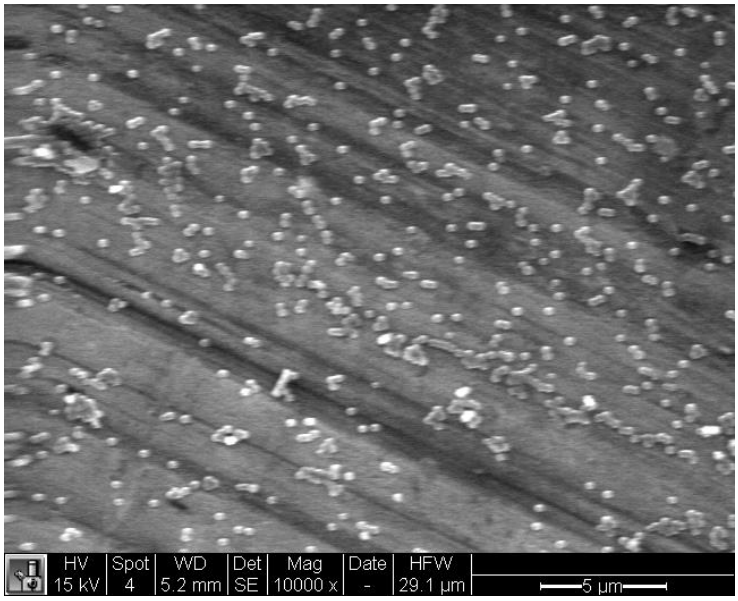

Figure 3-9: SEM image analysis of Experiment 2 Sample 3 shows many silica nanoparticles in the effluent.

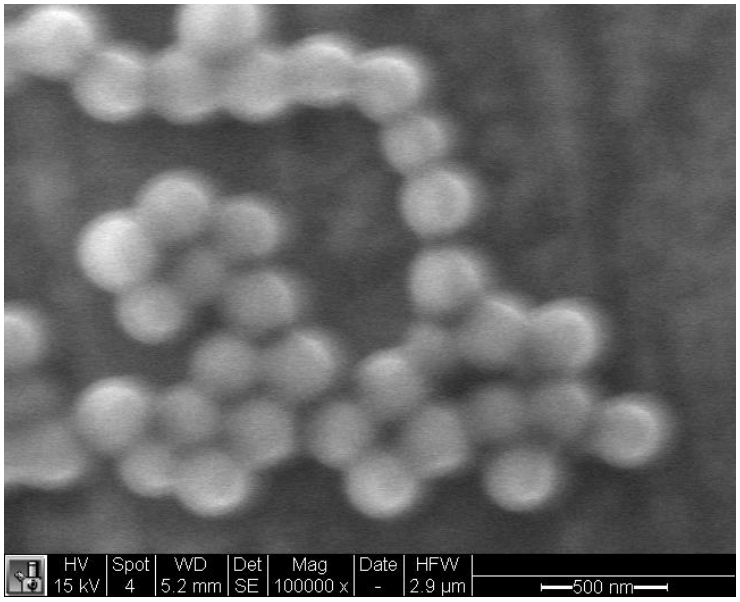

Figure 3-10: SEM image analysis of Experiment 2 Sample 4 shows spherical silica nanoparticles in the appropriate size range.

Experiment 3 was conducted at a temperature of 150°C and a flow rate of 2.50 mL/min. Sand pack baseline permeability was determined to be 40 darcy. Samples were taken periodically and evaluated using SEM image analysis. The differential pressure remained equivalent to the baseline permeability and eventually dropped below, increasing the permeability. The stabilized permeability after nanoparticle injection was calculated to be 44 darcy, an 11% increase.

It is believed that the higher temperatures accelerated the dissolution of sand grains inside the porous medium. Deionized water was also believed to accelerate dissolution, as it is known to be more chemically aggressive than geothermal reservoir fluids (Brinton et al., 2011).

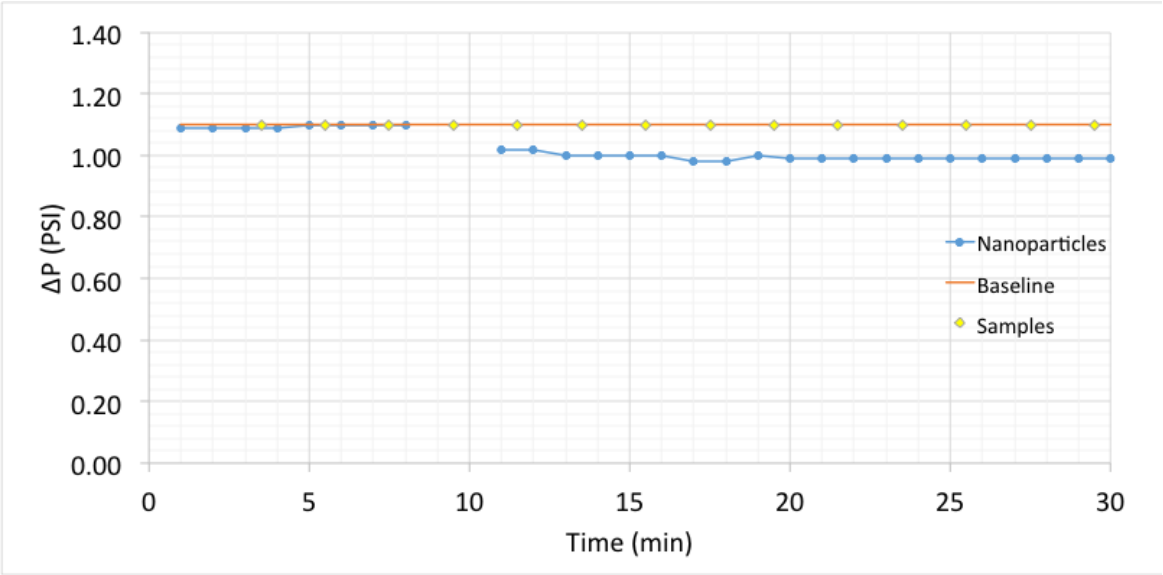

Figure 3-11: Experiment 3 plot of differential pressure vs. time. The orange line is the baseline differential pressure for water only, and was drawn for illustration purposes. The blue line represents measurements of differential pressure after silica nanoparticle injection. Sampling times are marked by golden diamonds.

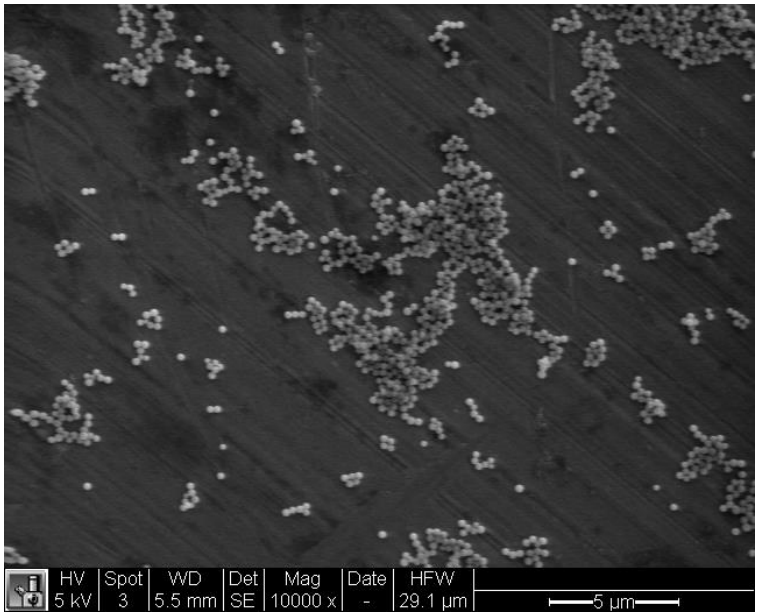

Figure 3-12: SEM image analysis of effluent from Experiment 3 Sample 2. This was the first sample to detect nanoparticles.

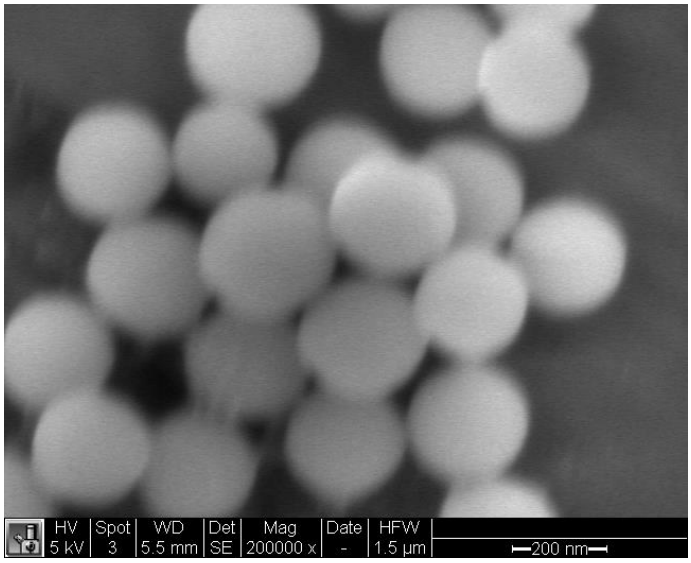

Figure 3-13: SEM image analysis of effluent from Experiment 3 Sample 2. Note that the spherical shape is maintained and the size is consistent with influent.

The purpose of these experiments was to study the transport of the particles through porous media and the effect of temperature upon particle integrity. In order to separate permeability effects due to sand pack dissolution from that of nanoparticle injection, further experimentation included a parallel experiment using only water. In this way the dissolution effects would be almost identical, allowing one to compare the effect of silica nanoparticle injection.

3.3.2. Injection with 1 hour residence period (Experiments 4-5)

Using the same apparatus, silica nanoparticles were injected into the sand pack at 150°C and held for a 1 hour period before being flowed out as effluent. Differential pressure was monitored and effluent samples were taken for SEM image analysis.

Using differential pressure data from Experiment 2, it was determined that the particles reached the sand pack approximately 5 minutes after the three-way valve was turned for injection. In experiments 4-5 the pump was paused five minutes after injection and the apparatus was sealed. System pressure was maintained for 1 hour. Following this residence period, the pump was restarted and run for 25 minutes. Differential pressure readings and samples resumed until the completion of the experiment.

In Experiment 4 the silica nanoparticle slug was injected at a temperature of 150°C and a flow rate of 2.50 mL/min. Sand pack baseline permeability was determined to be 48 darcy. Samples were taken periodically and evaluated using SEM image analysis. Following the 1 hour residence period, the differential pressure rose above baseline and then dropped below, increasing the permeability. The stabilized permeability after nanoparticle injection was calculated to be 58 darcy, a 20% increase.

Experiment 5 injected only water at a temperature of 150°C and a flow rate of 2.50 mL/min. Sand pack baseline permeability was determined to be 46 darcy. Following the 1 hour residence period, the differential pressure dropped below baseline and leveled off, increasing the permeability. The stabilized permeability after nanoparticle injection was calculated to be 67 darcy, an 46% increase.

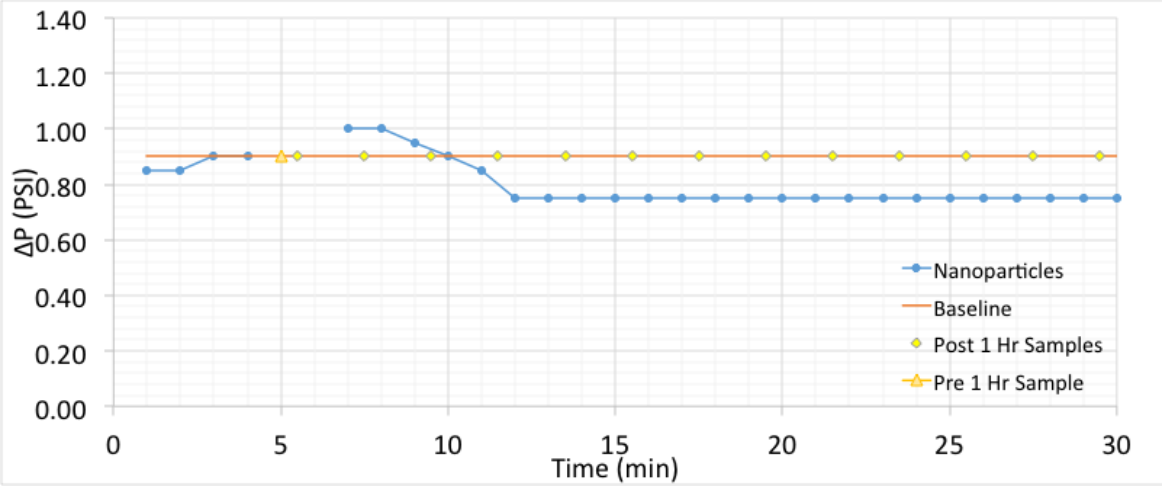

Figure 3-14: Experiment 4 plot of differential pressure vs time. The orange line is the baseline differential pressure for water only, and was drawn for illustration purposes. The blue line represents measurements of differential pressure after silica nanoparticle injection. Sampling times are marked by golden diamonds. The triangle at the 5 minute mark identifies the point where flow was halted for 1 hour.

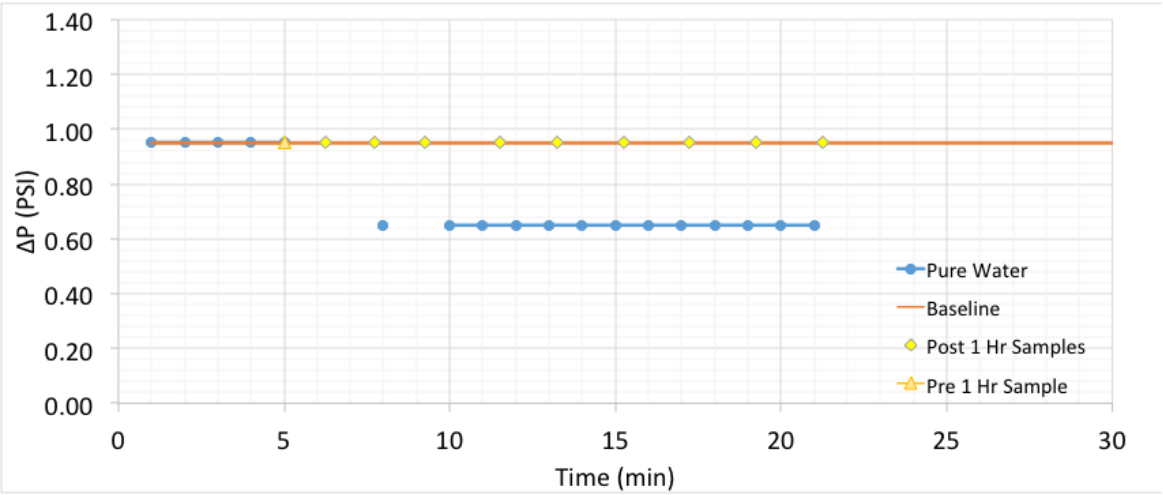

Figure 3-15: Experiment 5 plot of differential pressure vs time. Only water was injected to allow comparison with Experiment 4. Sampling times are marked by golden diamonds. The triangle at the 5 minute mark identifies the point where flow was halted for 1 hour.

Effluent samples from experiment 4 indicate that particle integrity was maintained. However, very small diameter (<10 nm) silica precipitate was observed in the later time samples. It is considered that dissolved silica precipitated out of solution when the fluid was cooled after entering the water pocket.

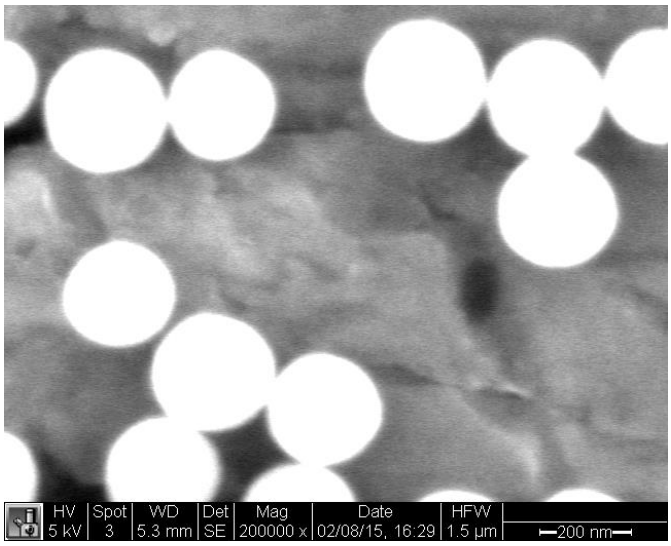

Figure 3-16: SEM image analysis for Experiment 4 Sample 2. Note that the spherical shape of the silica nanoparticle is maintained and the size is consistent with the influent.

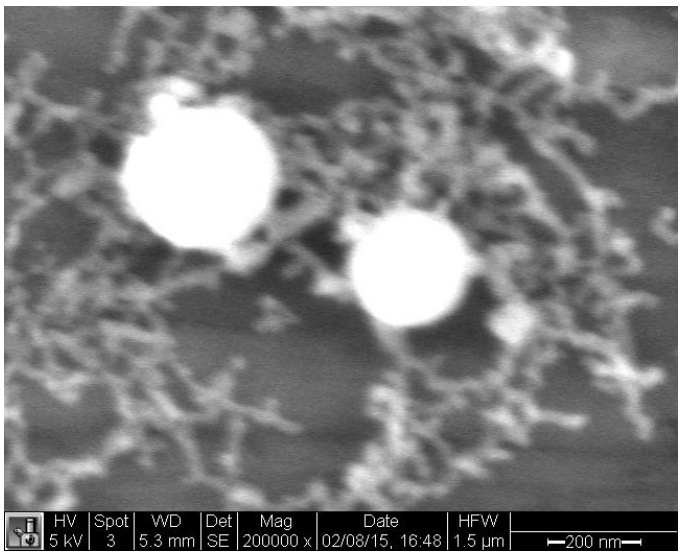

Figure 3-17: SEM image analysis for Experiment 4 Sample 7. Note the presence of amorphous silica, which was common among later samples. This is presumed to be dissolved silica that precipitated out of solution when the fluid was cooled in the water pocket. Also note that particle integrity is maintained.

Experiments 4-5 demonstrated that the silica nanoparticles could withstand the 150°C temperatures for an hour and still flow successfully through the sand pack. SEM image

analysis confirmed that the shape and size of the particles was consistent with the influent. Comparison between the water only and silica nanoparticle injection experiments show that the use of nanoparticles negatively impacts permeability. The water only experiment showed a permeability increase of 46%, but the nanoparticle injection experiment had only a 20% increase.

3.3.3. Injection with 6 hour residence period (Experiments 6-7)

For these experiments, silica nanoparticles were injected into the sand pack at 150°C and held for a 6 hour period before being flowed out as effluent. This was the only time the same sand pack was used for both experiments. The first injection was water only and the second was with the nanoparticles. Differential pressure was monitored and effluent samples were taken for SEM image analysis.

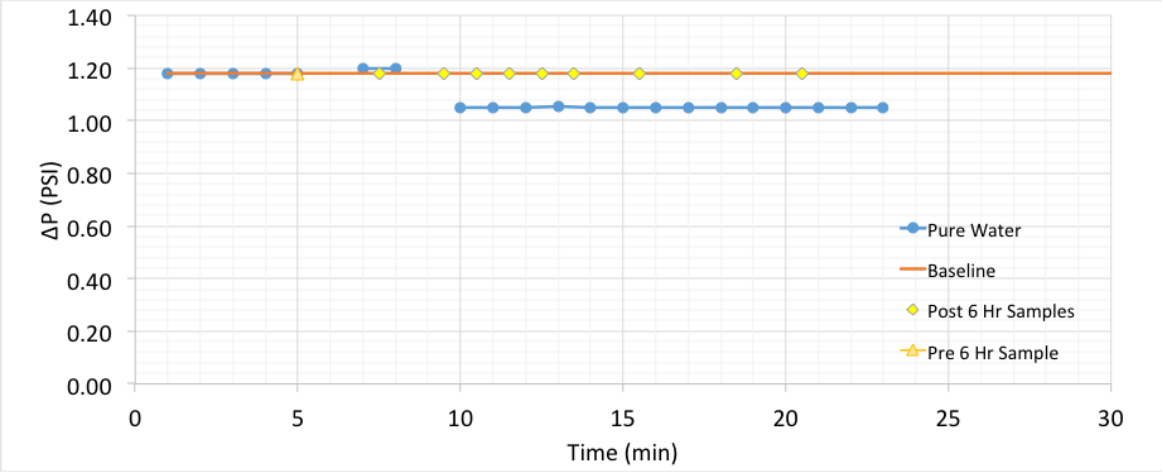

Figure 3-18: Experiment 6 plot of differential pressure vs time. Only water was injected to allow comparison with Experiment 7. Sampling times are marked by golden diamonds. The triangle at the 5 minute mark identifies the point where flow was halted for 6 hours.

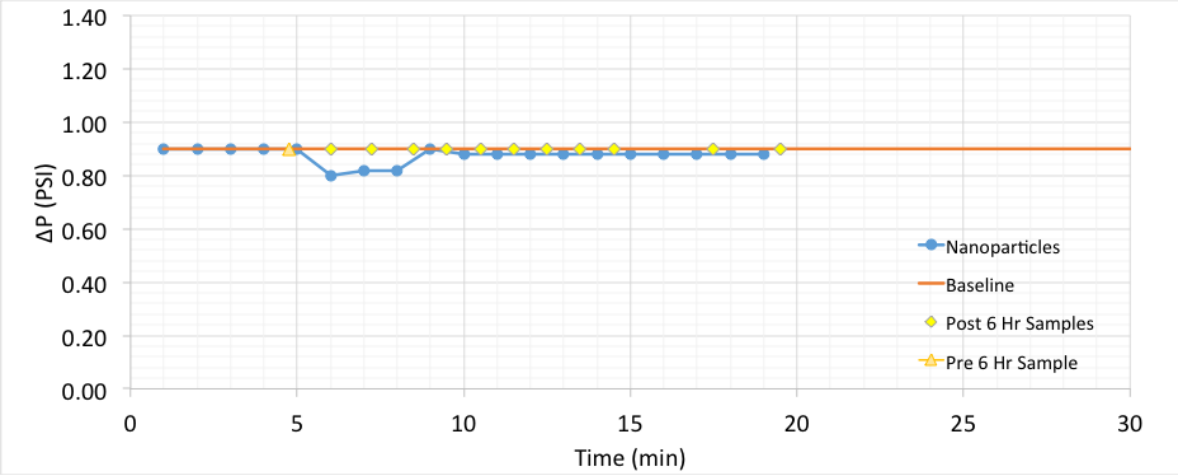

Figure 3-19: Experiment 7 plot of differential pressure vs time. Silica nanoparticles were injected and baked for 6 hours. Sampling times are marked by golden diamonds. The triangle at the 5 minute mark identifies the point where flow was halted.

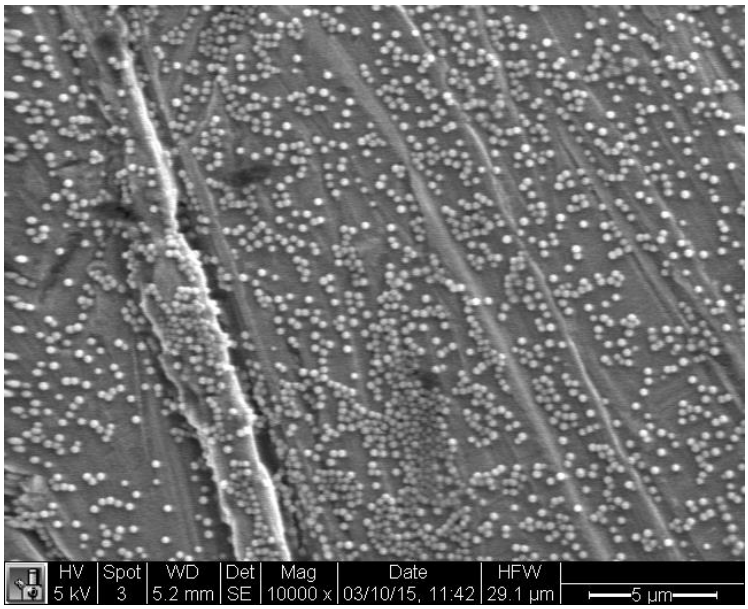

Figure 3-20: SEM image analysis for Experiment 7 Sample 4. A large number of silica nanoparticles clearly visible.

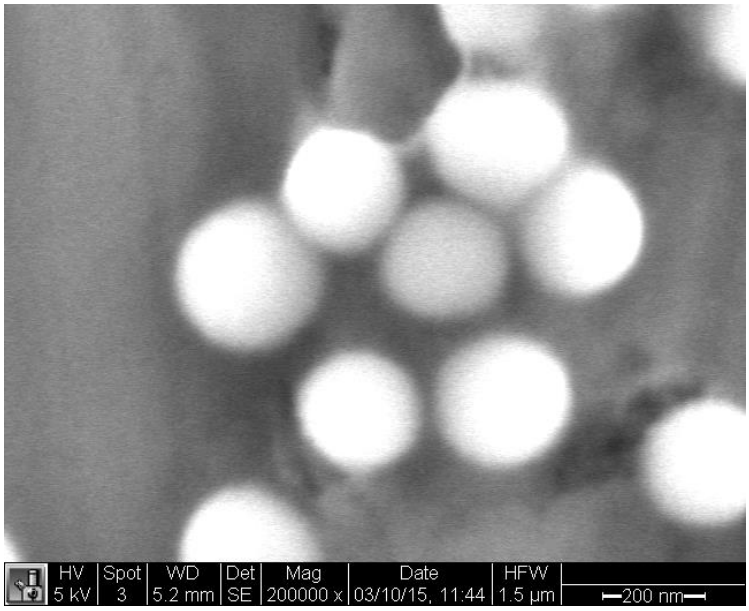

Figure 3-21: SEM image analysis for Experiment 7 Sample 4. Spherical shape, particle diameter and integrity appear maintained.

In order to investigate whether the sand pack permeability damage was a function of temperature, the apparatus was allowed to cool overnight and a "water flush" was conducted the next morning. The water pump was started and water was flowed through the sand pack at room temperature. Differential pressure was monitored and permeability calculations were made. In both experiments the calculated permeability was significantly higher than the baseline and post-injection permeabilities. It is believed that small bubbles of air trapped in the apparatus expanded under heat and restricted permeability. However, because the experiments were run sequentially on the same sand pack, the negative effect of the silica nanoparticles on permeability is clearly demonstrated.

Experiments 6-7 demonstrated that the silica nanoparticles could withstand the 150°C temperatures for 6 hours and still flow successfully through the sand pack. SEM image analysis confirmed that the shape and size of the particles was consistent with the influent. Comparison between the water only and silica nanoparticle injection experiments again confirmed that the use of nanoparticles negatively impacts permeability. The water only experiment showed a permeability increase of 12%, but the nanoparticle injection experiment had only a 2% increase.

3.3.4. Results of solid silica nanoparticle injection

Table 2 provides a summary of the Experiments 1-7. Note that permeability comparisons for the red and green shaded experiments were made between packed sand with either baseline water or nanoparticle suspension. Results indicate that in every case the nanoparticle suspension has a reducing effect on permeability. Experiment 3 shows an increase in permeability, but the following experiments confirmed that permeability was

increased in a purely water environment. However, permeability increased less when nanoparticles were injected.

Note that Experiments 1-5 each used a different set of packed sand, while Experiments 6-7 utilized the same sand. All flow rates were a constant 2.50 mL/min except for experiment 1 (1.20 mL/min).

The "water flush" was incorporated in Experiments 6-7 to investigate any change in permeability due to temperature. A significant change was noted, but the change was consistent in both experiments. Despite the effort to evacuate the apparatus with vacuum, it is believed that small bubbles of air expanded under temperature and had a reducing effect on permeability. Therefore at room temperature, the permeability was higher.

Despite the potential of air bubbles, the injected silica nanoparticles consistently demonstrated a reducing effect upon permeability.

Table 2: Solid silica nanoparticle injection experimental results

	Temperature	Experiment	Permeability [darcy]	Percent Change	Comments
1	25°C	Baseline Post-Silica Injection	54.0 49.2	-8.8	
2	120°C	Baseline Post-Silica Injection	93.0 85.9	-7.7	pH = 6.9 effluent
3	150°C	Baseline Post-Silica Injection	39.7 44.1	11.1	pH = 7.4 effluent
4	150°C	Baseline Post-1 Hour Bake	48.5 58.2	20.0	Silica Slug Injected
5	150°C	Baseline Post - 1 Hour Bake	45.9 67.1	46.2	Water Only
6	150°C 25°C	Baseline Post - 6 Hour Bake Water Flush	37.0 41.6 66.9	12.4	Water Only
7	150°C 25°C	Baseline Post - 6 Hour Bake Water Flush	48.5 49.6 70.8	2.3	Silica Slug Injected

3.4. DNA-embedded Silica Nanoparticle Injection Experiments

A final injection experiment was conducted to investigate whether simulated geological temperatures (150°C) combined with flow through porous media would adversely affect DNA-embedded silica nanoparticles.

These particles were prepared by labmate Yuran Zhang (Zhang, 2015). Unlike the solid silica spheres used in prior experiments, these particles were aggregated in clusters and subsequently coated with a silica shell. This is primarily due to the nature of the DNA

adsorption process, which utilizes negatively charged DNA and positively charged silica to pull the two materials together.

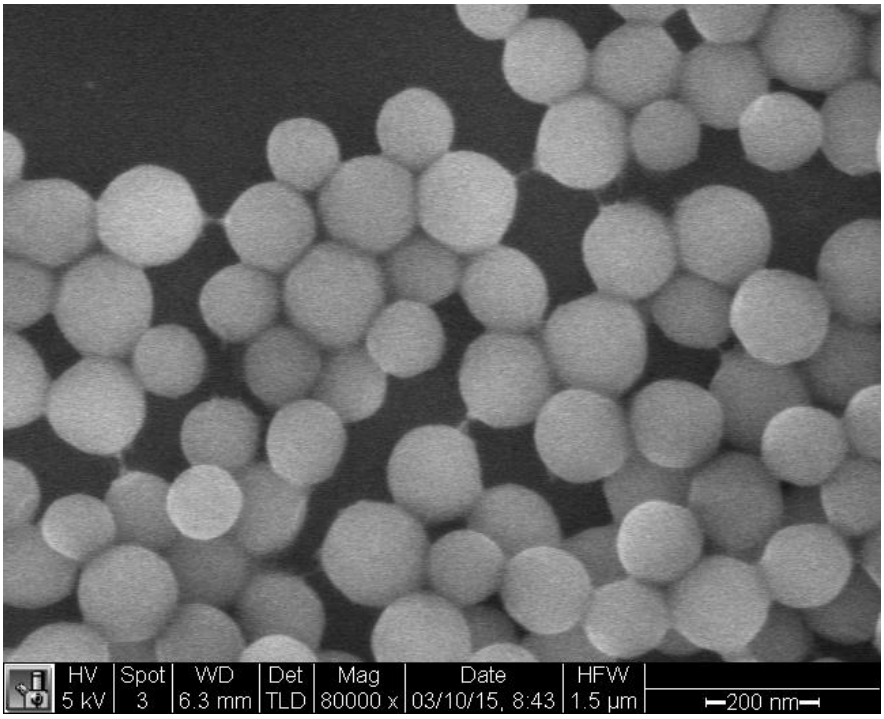

Figure 3-22: SEM image analysis depicting the effect of negatively charged synthetic DNA adsorbing to multiple positively charged silica nanoparticles. The subsequent silica coating will cover clusters of nanoparticles unless this issue can be resolved. Image reproduced from Zhang (2015).

Research is currently underway to eliminate the aggregation issue, which was known to Paunescu et al. (2012, 2013) but did not affect their intended use for the particles.

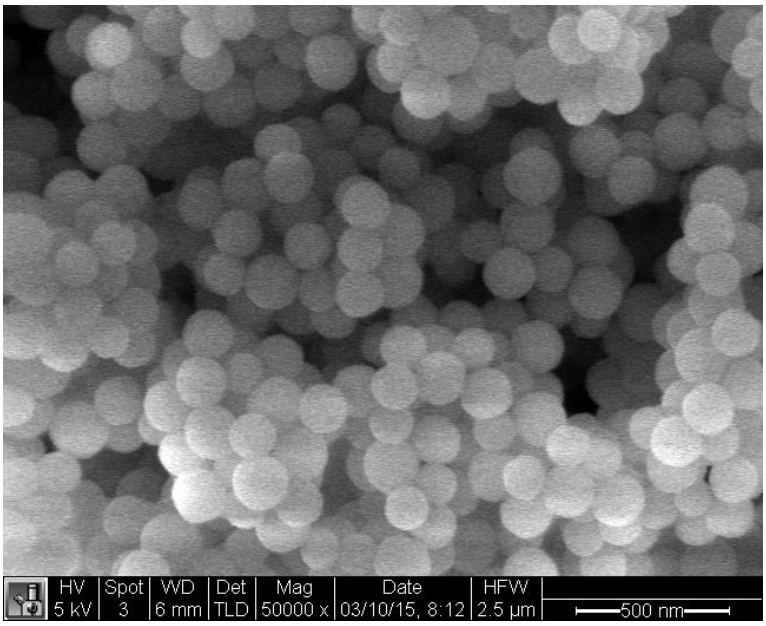

Figure 3-23: SEM image analysis of DNA-embedded silica nanoparticles prior to injection experiments. Note the particle clusters of multiple ~150 nm diameter nanoparticle spheres. Reproduced from Zhang and Manley, 2015.

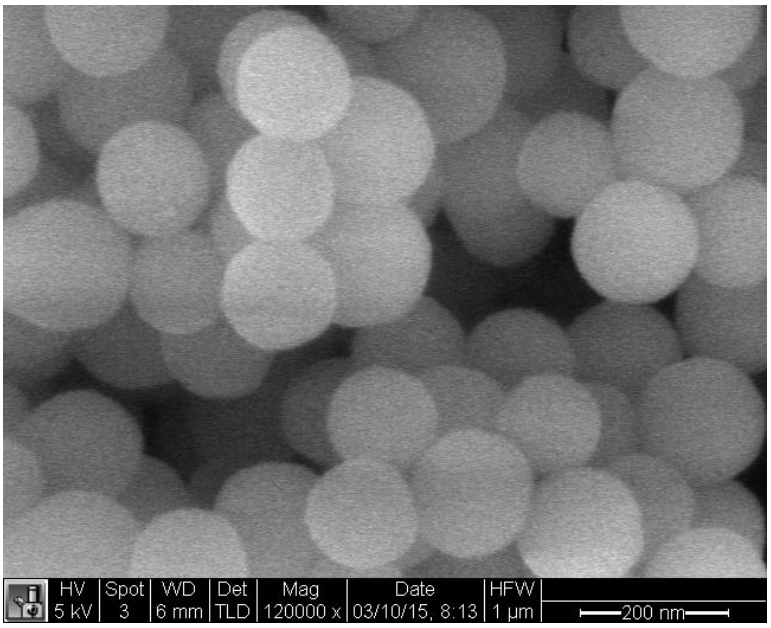

Figure 3-24: SEM image analysis of DNA-embedded silica nanoparticles prior to injection experiments. Note the particle clusters of multiple ~150 nm diameter nanoparticle spheres. Reproduced from Zhang and Manley, 2015.

It was therefore anticipated that the particles would have a more difficult time flowing through the sand pack due to their nonspherical shape as clusters. The goal of the

experiment was to determine if the synthetic DNA could survive the stresses of heat and flow through porous media, which would be confirmed in a successful qPCR DNA amplification (Zhang, 2015).

A new sand pack was prepared and the injection experiment was conducted with a flow rate of 2.50 mL/min. Unfortunately the differential pressure gauge failed, eliminating the ability to monitor permeability changes. The effluent, however, was regularly sampled and subjected to SEM image analysis.

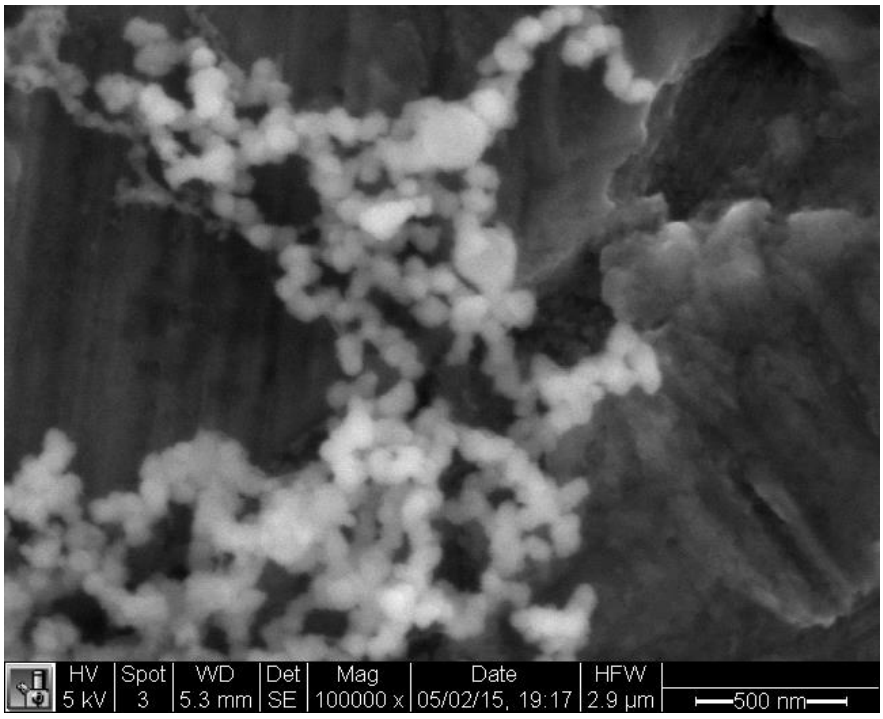

Figure 3-25: SEM image analysis of DNA-embedded nanoparticle injection effluent (Sample 4). The shape appears spherical but the diameter is much less than the influent. Particles this small are unlikely to be part of the influent, but more likely dissolved silica which has precipitated out of solution following the temperature reduction in the water pocket.

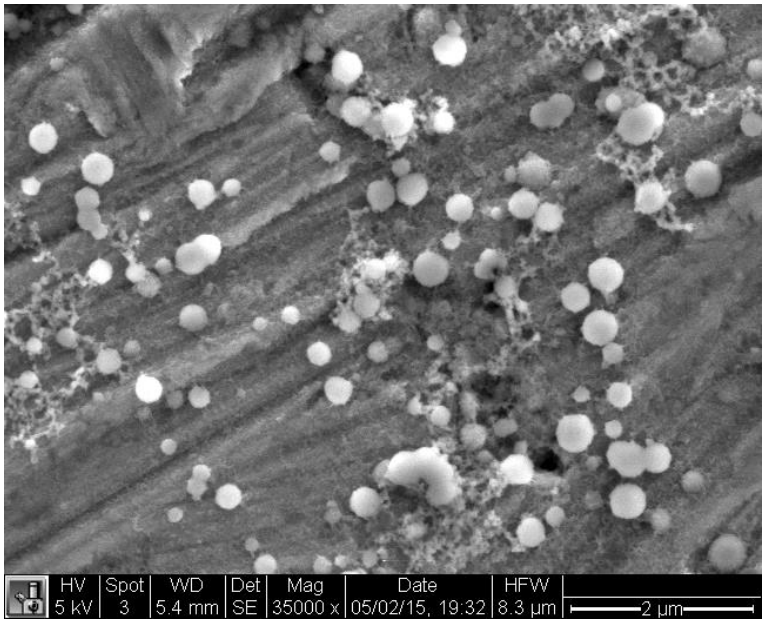

Figure 3-26: SEM image analysis of DNA-embedded nanoparticle injection effluent (Sample 6). An assortment of spherical nanoparticles are observed in the size range of the influent. Note the additional presence of silica precipitate from Figure 3-25.

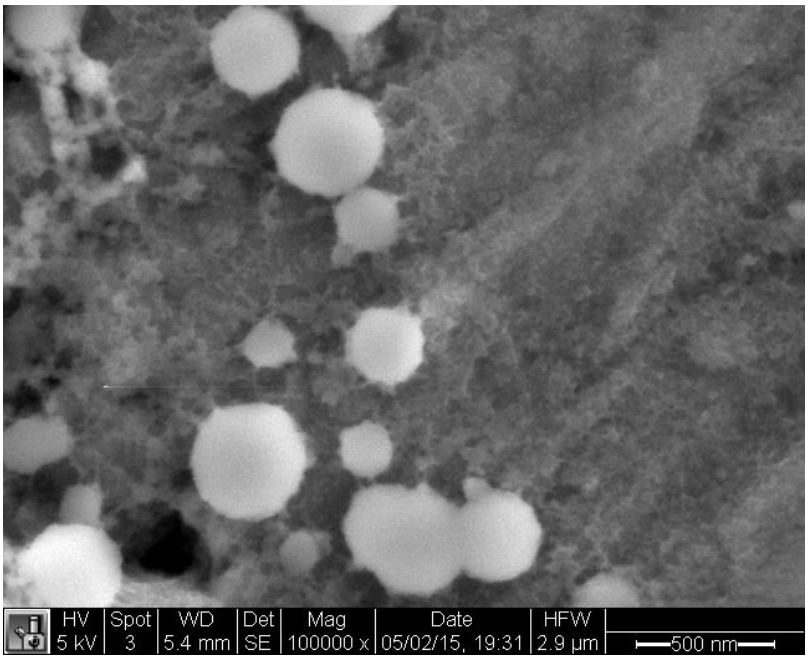

Figure 3-27: SEM image analysis of DNA-embedded nanoparticle injection effluent (Sample 6). This image is a magnified region from Figure 3-26. Variable degrees of dissolution are observed, but many particles appear sufficiently intact to protect the DNA.

While the particles were observed to have successfully traveled through the sand pack, the number of particles observed was significantly lower than in previous experiments. Due to differences in the nature of preparation, the surface charge of the DNA-embedded silica nanoparticles may be different from that of the solid silica nanoparticles (Zhang and Manley, 2015). Interactions between the particles and the sand grains could result in an attraction that resists transport.

It was also observed that the DNA-embedded silica nanoparticles fell out of suspension much more quickly than their solid silica counterparts. A stronger gravitational effect would also hinder particle transport, both through the porous media and the experimental apparatus.

Zhang (2015) conducted a qPCR analysis on the particles retrieved in the effluent. Results indicated insufficient DNA for amplification.

3.5. Interpretation and Discussion

Solid silica nanoparticles had a consistent reducing effect on the permeability of the packed sand. Though the deionized water appeared to have dissolved sand grains and increased permeability of the sand pack under heat, parallel experiments demonstrated that permeability increased less when silica nanoparticles were injected. Water flush experiments at room temperature demonstrated a consistent increase in permeability at room temperature following a heating experiment. It is believed that despite efforts to evacuate the apparatus using vacuum, small air bubbles remained and expanded under 150°C temperatures to reduce the sand pack permeability. Parallel experiments with the same sand pack demonstrated that this effect was consistent regardless of silica nanoparticle injection.

Samples were collected and subjected to SEM image analysis, which indicated that the solid silica nanoparticles had generally maintained their integrity and size. The most severely affected particles were observed to come much later than the “breakthrough” samples, which perhaps indicate retention and prolonged dissolution in the sand pack.

DNA-embedded silica nanoparticles were flowed successfully through the sand pack, although permeability was not able to be monitored. Samples were collected and analyzed using SEM image analysis. The quantity of nanoparticles in the effluent was much lower than in experiments with solid silica nanoparticles. The size distribution of effluent particles indicate variable dissolution, with some particles severely affected. These findings appear consistent with those of Alaskar (2013), who conducted an almost identical experiment at 150°C using DNA-embedded silica nanoparticles and observed size reduction by an approximate factor of four. Alaskar, however, did not observe particle size reduction or aggregation in experiments at room temperature.

The DNA-embedded silica nanoparticles are not identical to solid silica nanoparticles, and these differences may have been contributing factors to the varying injection results. The DNA-embedded particles appeared to fall out of suspension more quickly, which indicate

a higher density and vulnerability to gravity settling. The process pioneered by Paunescu et al. (2012) for synthesis of DNA-embedded silica nanoparticles utilized the difference in charge between silica and synthetic DNA to adsorb the DNA and coat the particle. These processes may affect the particle surface charge, thereby altering the manner in which the particles interact with the porous media and perhaps encouraging retention.

It is also possible that most of the particles never flowed to the packed sand, but were retained in the slug chamber or along the route to the porous media due to gravitational settling. Investigation is underway to determine if a large quantity of nanoparticles became trapped at the inlet to the packed sand or settled along the route.

Chapter 4

4. Conclusions and Recommendations for Future Work

Solid silica nanoparticles were evaluated for integrity and flow characteristics under simulated geological conditions.

Although dissolution and aggregation were present in the controlled heating experiments, the particles appeared to maintain a size and shape consistent to their preheated state. The 200 nm particles appeared to have undergone some degree of dissolution, though it was not severe. The presence of deionized water likely accelerated any dissolution, as it is known to have a chemically aggressive effect compared to geothermal fluids (Brinton et al., 2011).

Injection experiments of solid silica nanoparticles through packed sand at 25, 120 and 150°C demonstrated favorable flow characteristics, though a reducing effect upon permeability was observed. Samples collected and analyzed from the effluent indicated that particle integrity was maintained.

DNA-embedded silica nanoparticles were flowed through packed sand at 150°C and observed in the effluent. Variable dissolution was observed, which was in some cases severe, and the overall number of particles retrieved was significantly lower. These results are consistent with Alaskar (2013), who observed a reduction in size of an approximate factor of four. A qPCR analysis was conducted by Zhang (2015) on the effluent, and insufficient DNA was present for amplification.

4.1. Conclusions

Silica nanoparticles have proven to be a particle tracer worthy of further investigation.

In every experiment, the silica nanoparticles maintained their original spherical shape, which has been identified as an ideal shape for transport through porous media (Alaskar, 2013). While smaller particles were more vulnerable to dissolution, the degree of dissolution was not considered severe except in some of the DNA-embedded particles.

The solid silica particles demonstrated excellent flow characteristics, and were identified in large numbers in the effluent. The DNA-embedded silica particles, while greatly reduced in number, were still visible in the effluent. Further research and experimentation is underway to address the issue of particle clustering, variable dissolution and apparent retention in the sand pack.

Given the low detection limit of qPCR, DNA-embedded silica nanoparticles display promise as a uniquely identifiable tag for a variety uses in geothermal and petroleum applications (Zhang and Manley, 2015).

4.2. Recommendations for future work

There is a multitude of factors that affect particle transport through porous media. Current experimentation has indicated that particles with certain features tend to flow more easily.

The process pioneered by Paunescu et al. (2012) utilizes silica as the material for DNA adsorption and coating. Zhang (2015) successfully repeated this process to develop DNA-embedded silica nanoparticles with an average diameter around 150 nm, although clustering was evident. Similar aggregation was observed by Puddu et al. (2014) but was not addressed, as their purpose was not to flow the particles through porous media. Further work is needed to address the issue of aggregation prior to adding the outer silica shell.

Size is another important factor in particle mobility. In the case of this research, the pore throats of the sand pack were sufficiently large to mitigate plugging due to size alone. Bridging, however, remains a possibility due to the high concentration of injected particles. For traditional reservoir media, clustered particles would not be sufficient for tracer operations. A smaller nanoparticle would still be large enough to avoid the vulnerability to diffusivity, while also reducing effects of gravitational settling or straining (Cumbie and McKay, 1999).

The surface charge of the particle is another factor that could be adjusted to lower particle retention in porous media. Recent experiments with a variety of nanoparticles have indicated that particles with a near zero zeta potential show the least retention in calcium carbonate, which had a zeta potential peak of -14.5mV in deionized water and +1.0mV in oil field brine (Li et al., 2014). Zhang (2015) attempted to measure the zeta potential of the DNA-embedded silica nanoparticles injected through packed sand, but the data was noisy and inconclusive. The solid silica nanoparticles, however, were measured to have an average zeta potential of -50mV. Those used as the core for DNA-embedded silica nanoparticles underwent surface functionalization, which resulted in a +40mV zeta potential (Zhang and Manley, 2015). The large shift in surface charge could be a contributing factor in particle retention for the DNA-embedded nanoparticles.

The most important factor, however, affecting zeta potential is pH.[7] Adding acid or alkali to a suspension would raise or lower the zeta potential from its previous state.[8] A typical plot of potential versus pH is shown in Figure 4-1.

[7] *Zetasizer Nano Series User Manual*. MAN0317 Issue 1.1. Feb. 2004. p 15.2.

[8] *Zetasizer Nano Series User Manual*. MAN0317 Issue 1.1. Feb. 2004. p 15.2.

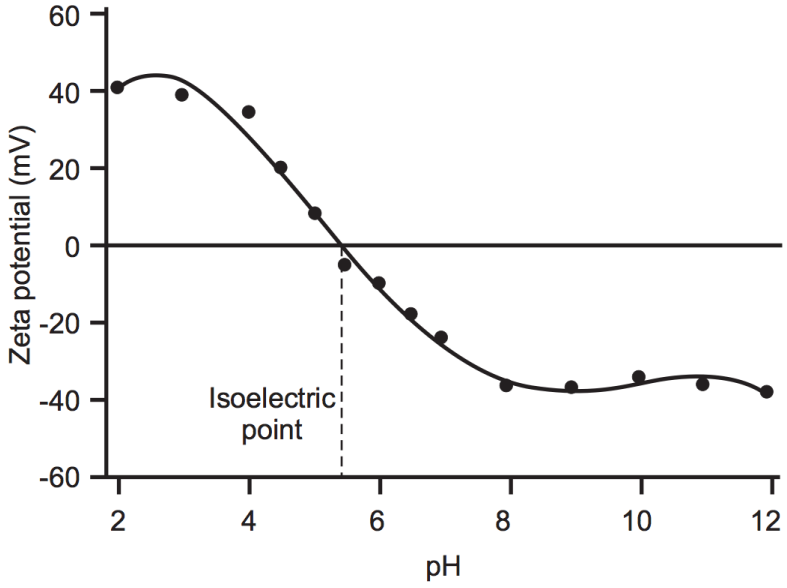

Figure 4-1: The isoelectric point is defined as the point where the plot passes through zero zeta potential. The isoelectric point is also considered a point of least stability for a colloidal system.[9] Reproduced from *Zetasizer Nano Series User Manual*. MAN0317 Issue 1.1. Feb. 2004.

Nanoparticles have also exhibited more favorable flow characteristics in a suspension that is slightly acidic compared to basic. Varying concentrations of bentonite suspended in synthetic silica solution of 700ppm at 80°C were flowed through sand packs in basic (pH 8) and acidic (pH 5.5) conditions (Tusara et al, 2014). Permeability was monitored, and the permeability drop was observed to be less severe in the acidic experiments.

In order to reduce interactions between nanoparticles and the porous media, some researchers have added highly hydrophilic polymer hairs to nanoparticle cores, which extend from the particle and buffer it from close contact with the rock surface (Li et al., 2014; Subramanian et al., 2013). Such a feature was identified to be consistent with higher levels of particle recovery.

Coating the nanoparticle is another possibility to reduce the effect of electrostatic interaction causing particle aggregation and attachment to rock surfaces. Rodriguez et al. (2009) injected 5 and 20 nm solid silica nanoparticles coated with a ~5nm thick polymer through a variety of cores with great success. Sandstone and limestone cores had similar returns though the charges were opposite, indicating that the coating effectively shielded the nanoparticles from surface charge effects (Rodriguez et al., 2009).

Therefore based upon the results of this research and existing research elsewhere, the DNA-embedded silica nanoparticle should continue to be developed and modified to flow through porous media. There are many modifications that look promising and should be explored, such as hydrophilic polymer hairs, coating, size reduction, and adjustment of pH

[9] *Zetasizer Nano Series User Manual*. MAN0317 Issue 1.1. Feb. 2004. p 15.3.

and zeta potential. There is a great deal of interest in nanoparticles, across the entire spectrum of science, engineering and industry. Innovation is not far away when demand is high and many disciplines are engaged in a similar pursuit.

Nomenclature

AES = Auger Electron Spectroscopy

DLS = Dynamic Light Scattering

EDS = Energy dispersive X-ray spectroscopy

EGS = Engineered Geothermal Systems

HDR = Hot, Dry Rock

SEM = Scanning Electron Microscope

TEM = Transmission Electron Microscope

TEOS = tetraethyl orthosilicate

$q =$ volumetric flow rate

$t =$ time

$\Delta p =$ pressure drop across porous media

$L =$ length of flowpath

$A =$ flowpath cross sectional area

$\mu =$ liquid viscosity

$k =$ permeability of porous media

$\Gamma =$ decay constant

$\tau =$ time delay

$n =$ liquid refractive index

$\lambda =$ wavelength of laser light

$\theta =$ scattering angle

$q =$ scattering vector

$D_h =$ hydrodynamic diameter

$D_t =$ translational diffusion coefficient

$k_B =$ Boltzmann's constant

$T =$ thermodynamic temperature

$\eta =$ dynamic viscosity

References

Alaskar, M., Ames, M., Connor, S., Liu, C., Cui, Y., Li, K., and Horne, R. 2012. "Nanoparticle and Microparticle Flow in Porous and Fractured Media—an Experimental Study. SPEJ, 17, 1160-1171.

Alaskar M., 2013. "In-Situ Multifunctional Nanosensors for Fractured Reservoir Characterization." PhD thesis, Dept of Energy Resources Engineering, Stanford University

Ames M., 2011. "Nanosensors as Reservoir Engineering Tools to Map In-situ Temperature Distributions in Geothermal Reservoirs." Master thesis, Dept of Energy Resources Engineering, Stanford University

Bohlmann, E.G., Shor, A.J., Berlinski, P. 1976. "Precipitation and Scaling in Dynamic Geothermal Systems." Oak Ridge National Laboratory.

Brinker, C.J. and Scherer, G.W. 1990. *Sol-Gel Science: The Physics and Chemistry of Sol-Gel Processing*. San Diego: Academic Press Inc.

Brinton, D., K. McLin, J. Moore, 2011. "The Chemical Stability of Bauxite and Quartz Sand Proppants Under Geothermal Conditions." Thirty-sixth Workshop on Geothermal Reservoir Engineering, SGP-TR-191.

Cumbie, D.H. and McKay, L.D., 1999. Influence of diameter on particle transport in a fractured shale saprolite. J. Contam. Hydrol. 37 (1–2): 139–157. http://dx.doi.org/10.1016/s0169-7722(98)00156-9.

DLS Technical Note. "Dynamic Light Scattering: An Introduction in 30 Minutes." Malvern Instruments. MRK656-01.

Goa, B., J.E. Saiers, and J. Ryan, 2006. "Pore-scale mechanisms of colloid deposition and mobilization during steady and transient flow through unsaturated granular media." Water Resources Research. Vol. 42. W01410. doi: 10.1029/2005WR004233

Iler, R.K., 1979. *The Chemistry of Silica-Solubility, Polymerization, Colloid, and Surface Properties, and Biochemistry*. John Wiley & Sons, Inc., New York.

Ishibashi, T., Watanabe, N., Hirano, N., Okamoto, A., and Tsuchiya, N. 2014. "Beyond-laboratory-scale prediction for channeling flows through subsurface rock fractures with heterogeneous aperture distributions revealed by laboratory evaluation." *J. Geophys. Res. Solid Earth*, 120, 106-124, doi:10.1002/2014JB011555.

Kanj, M.Y., Funk, J.J., and Al-Yousif, Z. 2009. Nanofluid Coreflood Experiments in the ARAB-D. Presented at the SPE Saudi Arabia Section Technical Symposium, AlKhobar, Saudi Arabia, 9–11 May. SPE- 126161-MS. http://dx.doi.org/10.2118/126161-ms.

Kanj, M.Y., 2013. "Reservoir Nanoagents for In-Situ Sensing and Intervention." Ch. 4. *Nanorobotics*. Springer, New York. p. 51-67.

Li, Y.V., Cathles, L.M., Archer, L.A., 2014. "Nanoparticle tracers in calcium carbonate porous media." Springer Science+Business Media Dordrecht.

McLin, K.S., Moore, J.N., Hulen, J., Bowman, J.R., Berard, B. 2006. "Mineral Characterization of Scale Deposits in Injection Wells; Coso and Salton Sea Geothermal Fields, CA. Thirty-First Workshop on Geothermal Reservoir Engineering, SGP-TR-179.

Paunescu D., M. Puddu, J. Soellner, P. Stoessel, R. Grass, 2013. "Reversible DNA encapsulation in silica to produce ROS-resistant and heat-resistant synthetic DNA 'fossils'" Nature Protocols, v.8, p. 2440-2448.

Paunescu D., R. Fuhrer, R. Grass, 2012. "Protection and Deprotection of DNA—High-Temperature Stability of Nucleic Acid Barcodes for Polymer Labeling" Angewandte Chemie, v. 52, p. 4269-4272.

Paunescu, D., Puddu, M., Soellner, J., Stoessel, P., Grass, R., 2013. "Reversible DNA encapsulation in silica to produce ROS-resistant and heat-resistant synthetic DNA 'fossils'." Nature Protocols. Vol. 8. No. 12.

Puddu, M., Paunescu, D., Stark, W., Grass, R., 2014. "Magnetically Recoverable, Thermostable, Hydrophobic DNA/Silica Encapsulates and Their Application as Invisible Oil Tags." American Chemical Society.

Reimus, Paul W., 1995. "The Use of Synthetic Colloids in Tracer Transport Experiments in Saturated Rock Fractures." PhD thesis, University of New Mexico.

Rodriguez, E., Roberts, M.R., Yu, H., Huh, C., Bryant, S., 2009. "Enhanced Migration of Surface-Treated Nanoparticles in Sedimentary Rocks." Society of Petroleum Engineers. SPE 124418.

Subramanian, S.K., Li, Y., Cathles, L.M., 2013. "Assessing preferential flow by simultaneously injecting nanoparticle and chemical tracers." Water Resources Research. Vol. 49. p.29-42. doi:10.1029/2012WR012148.

Tusara, L., Itoi, R., Fukuda, D., Kawahara, Y. 2014. "Change in Permeability of Porous Medium in Silica Scaling Experiment under Different pH and Suspended Particle Concentration." Thirty-ninth Workshop on Geothermal Reservoir Engineering, SGP-TR-202

Zetasizer Nano Series User Manual. 2003, 2004. Malvern Instruments Ltd. MAN0317. Issue 1.1. Feb. 2004.

Zhang, Y., 2015. "DNA-Encapsulated Silica Nanoparticle Tracers for Fracture Characterization." Master thesis, Dept of Energy Resources Engineering, Stanford University.

Zhang, Y., Manley, T., Li, K., Horne, R., 2015. "DNA-Encapsulated Silica Nanoparticle Tracers for Fracture Characterization." Geothermal Resources Council.